Chapter 3
Fundamentals of Cutting

DIN 8580 defines machining as all process variants of the third main group "Cutting", in which form is altered by means of reducing material cohesion. Deformation is achieved by means of a relative motion between the tool and the workpiece that brings about a transfer of energy [DIN8580].

In the standard, this basic classification is further refined in order to categorise machining procedures [DIN8589]. Machining is defined as follows: cutting, in which layers of material are mechanically separated from a workpiece in the form of chips by means of a cutting tool. According to DIN 8580, machining comprises Groups 3.2 (machining with geometrically defined cutting edges) and 3.3 (machining with geometrically undefined cutting edges) in the manufacturing classification system.

The first part of this compendium on manufacturing processes deals exclusively with process variants of Group 3.2. For this reason, the term "machining" will only be used in the sense of cutting with geometrically defined cutting edges. What all processes in the group of geometrically defined cutting edges have in common is that they use a tool, of which the cutting edge number, geometry and position to the workpiece are determined.

Several concepts and terms are necessary to describe cutting part, which will be described in the following.

3.1 The Cutting Part – Concepts and Terms

The concepts, designations and terms used to describe the geometry of the cutting part are set down in DIN 6581. The cutting part is the active part of the tool where the cutting wedges are located with the cutting edges. The idealized cutting wedge is made up of two faces: A rake face and a flank face, which cut in a line, cutting edge S. The angle between these two faces is designated as the wedge angle β. Figure 3.1 shows an idealized cutting wedge [DIN6581].

The rake face A_γ is the face of the cutting edge where the chip runs off. The flank face A_α is the face on the cutting wedge, which is turned towards the new workpiece surface (the cut surface). These terms make it clear that the cutting wedge

F. Klocke, *Manufacturing Processes 1*, RWTH edition,
DOI 10.1007/978-3-642-11979-8_3, © Springer-Verlag Berlin Heidelberg 2011

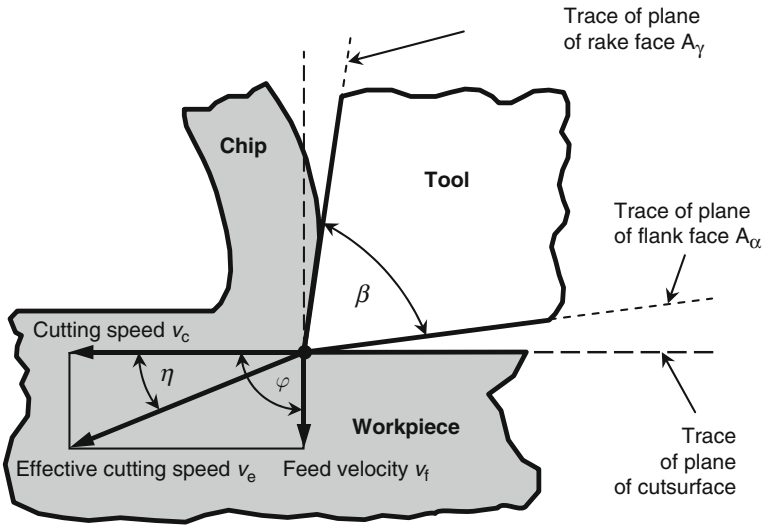

Fig. 3.1 Description of the idealized cutting wedge

(tool) should always be regarded in connection with the workpiece. This means that considerable importance should be attached to process kinematics.

One model concept is often used for the sake of a simplified description of process kinematics, that of the selected cutting point. This model simplifies the actual kinematics by summarizing the spatial velocity fields in one point, the selected cutting point. At the selected cutting point, the velocity fields can be represented in a summarizing fashion by means of vectors. These vectors can be summarized in turn by vector addition in one total vector. Usually, the workpiece is assumed to be fixed; all motions are carried out by the tool. The resulting velocity vector is designated as the effective cutting speed v_e. It can be divided into two components; the cutting velocity v_c in the cutting direction and the feed velocity v_f in the feed direction. To position the components of effective cutting speed clearly, two angles are defined:

- The effective cutting speed angle η as the angle between the effective cutting direction and the direction of primary motion (see Fig. 3.1)
- The feed motion angle φ as the angle between the feed direction and the direction of primary motion (see Fig. 3.1)

Since there are no ideally sharp tools in practice, cutting edge rounding is taken into consideration (Fig. 3.2).

In almost all cases the transition between flank and rake face is curved. This curvature is described by the cutting edge radius r_β.

Up to this point, the concepts have been explained using a simple cutting wedge formed by two faces. Generally, more complex tools are used, composed of several cutting wedges, in the simplest case of one major cutting wedge and one minor cutting face (Fig. 3.3).

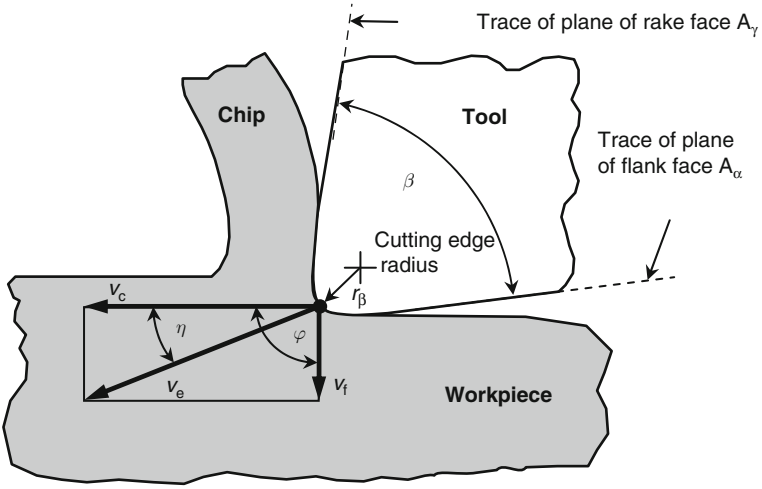

Fig. 3.2 Cutting edge with cutting edge radius

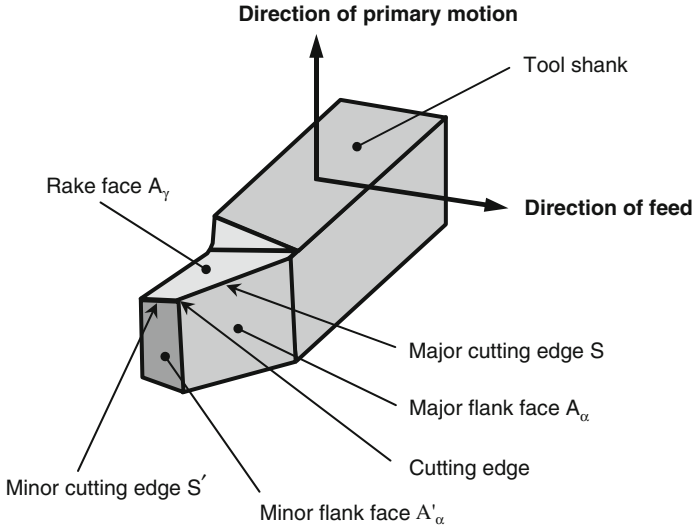

Fig. 3.3 Cutting edges and faces of the wedge, acc. to DIN 6581

Correspondingly, we speak of major and minor cutting edges. The major cutting edge S is always turned towards the cut surface, the minor cutting edge S' towards the machined face [DIN6580]. If the selected cutting point is on the minor cutting edge, the concepts defined in the former are named accordingly and furnished with an apostrophe ($'$). The flat areas of the major and minor cutting edges are joined by the corner radius r_ϵ (Fig. 3.6).

3.2 Reference Systems

In order to describe the location, position and direction of motion of a cutting wedge, reference systems are utilized in which characteristic planes are defined that are valid for all process variants.

The two standardized reference systems are the tool-in-hand system and the tool-in-use system (Fig. 3.4). The tool-in-hand system was developed for tool design as well as for the production and testing of cutting tools. In the tool-in-hand system, the tool angle is measured without considering process kinematics. In actual cutting processes however, the effective angle deviates from the nominal tool angle under certain circumstances due to process kinematics (exception: the wedge angle). For this reason, a tool-in-use system is also defined (Fig. 3.4, right).

The tool-in-hand system is a system, the reference plane of which is oriented orthogonally to the assumed cutting direction. In contrast, the reference plane of the tool-in-use system is oriented orthogonally to the effective direction. In both systems, all planes contain the selected cutting point. The reference systems are in agreement when the cutting direction corresponds to the effective direction.

First, the tool-in-hand system will be considered (Figs. 3.4, left, and 3.5):

- The basic plane, upon which all other planes are based, is the tool reference plane P_r. It contains the rotation axis (if present) and lies perpendicularly to the assumed cutting direction.

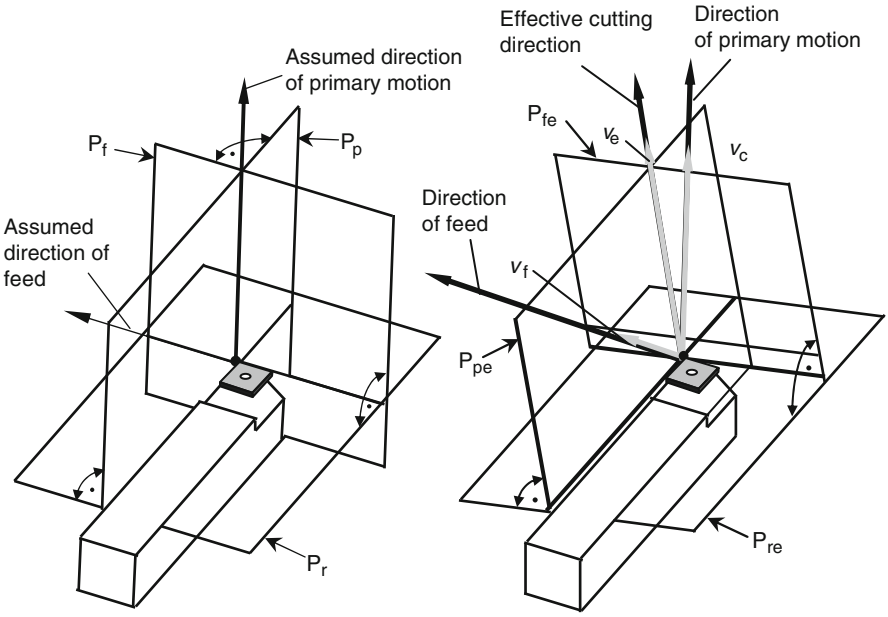

Fig. 3.4 Tool frame of reference (*left*) and tool-in-use system, acc. to DIN 6581

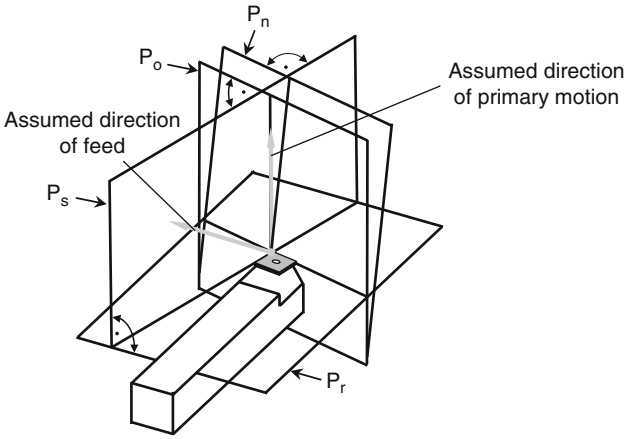

Fig. 3.5 Orientation in tool frame of reference

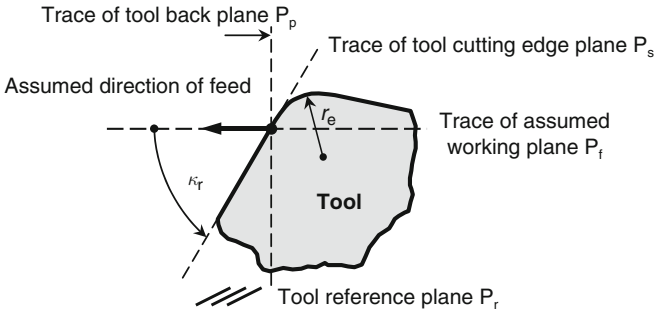

Fig. 3.6 Position of tool cutting edge angle κ_r

- The cutting edge plane P_s runs tangentially to the cutting edge S and perpendicularly to the tool reference plane P_r.
- The tool orthogonal plane P_o is perpendicular to the tool cutting edge plane P_s.
- The assumed working plane P_f is perpendicular to the tool reference plane P_r and parallel to the assumed feed direction.
- The tool back plane P_p stands perpendicularly on the tool reference plane P_r and perpendicularly on the assumed working plane P_f.
- The tool cutting edge normal plane P_n is perpendicular to the cutting edge S. The tool cutting edge normal plane P_n is identical to the effective cutting edge normal plane P_{ne}, since it is not oriented to the tool reference plane but rather to the major cutting edge.

The tool-in-use system is rotated towards the tool-in-hand system by the effective cutting speed angle η. In tool-in-use system, the same signs are used as in tool-in-hand system; they are followed however by an e, which stands for "effective".

In order to designate all tool and effective angles clearly, the same index is assigned to them that signifies the plane in which these angles are measured. For example, the tool orthogonal wedge angle β_o is measured in the tool orthogonal plane P_o, or the effective side rake angle γ_{fe} is measured in the working plane P_{fe}.

Information about three angles around the three rotatory axes in space is required in order to determine the orientation of the cutting edges or the positions in space of the rake and flank faces. For an optimal cutting process, certain orientations are responsible for three rotatory axes in space. In the following, these angles will be explained exemplarily in the tool-in-hand system:

- the orientation angle around a rotation axis that stands orthogonally on the tool reference plane P_r:
  The tool cutting edge angle κ_r between the tool cutting edge plane P_s and the assumed working plane P_f, measured in the tool reference plane P_r, is defined as the angle that determines the position of the major cutting edge S in the tool reference plane P_r. It is measured mathematically positively on the basis of the assumed working plane P_f (Fig. 3.6).
- the orientation angle around a rotation axis that stands orthogonally on the tool cutting edge plane P_s:
  The tool cutting edge inclination λ_s between the major cutting edge S and the tool reference plane P_r, measured in the tool cutting edge plane P_s, is defined as the angle that determines the position of the major cutting edge S in the tool cutting edge plane P_s (Fig. 3.7).
- the orientation angle around a rotation axis that stands orthogonally on the tool cutting edge normal plane P_n:
  This rotation is executed by one of the tool angles α_n or γ_n, which are measured in the tool cutting edge normal plane P_n. The tool normal rake angle γ_n is customarily used as the orientation angle, as it has a large effect on the cutting process (Fig. 3.8).

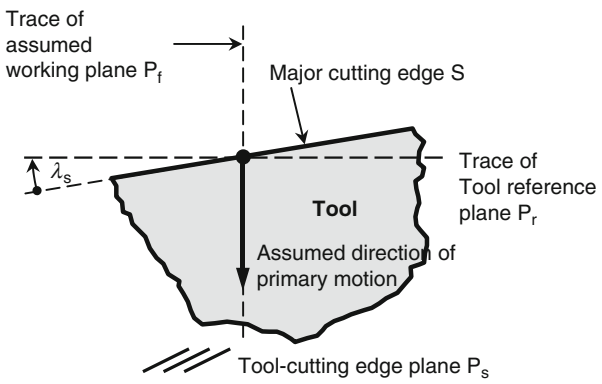

Fig. 3.7 Position of cutting edge inclination λ_s

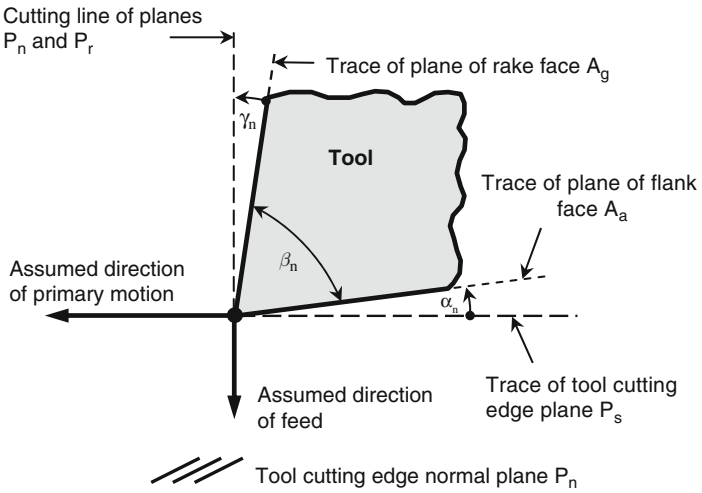

Fig. 3.8 Position of wedge in tool frame of reference

It is measured mathematically positively between the tool rake face A_γ and the tool reference plane P_r in the tool cutting edge normal plane P_n. The tool normal wedge angle β_n is always fixed on the tool and cannot be changed by tool rotation. The tool normal orthogonal clearance angle α_n lies between the tool flank face A_α and the tool cutting edge plane P_s, measured in the tool cutting edge normal plane P_n.

The angle between the flank face A_α and the tool cutting edge plane P_s, measured in the tool orthogonal plane P_o, is designated as the tool orthogonal clearance angle α_o. The angle between the rake face A_γ and the tool reference plane P_r is defined as the tool orthogonal rake angle γ_o. The angle between the rake face A_γ and the flank face A_α is called the tool orthogonal angle β_o. As rule, the clearance angle, wedge angle and rake angle – defined in the tool orthogonal plane $\mathrm{P_o}$, the assumed working plane $\mathrm{P_f}$ and the tool cutting edge normal plane $\mathrm{P_n}$ – must in total make a 90° angle.

The kinematic factors of tool cutting edge angle κ_r, tool cutting edge inclination λ_s and tool normal rake angle γ_n are important influencing parameters on the cutting process. For further information, see DIN 6582.

3.3 Basic Process Variants

Despite the large number of cutting process variants, they can still all be subdivided into three main categories:

- free, orthogonal cuts,
- free, diagonal cuts and
- bound, diagonal cuts.

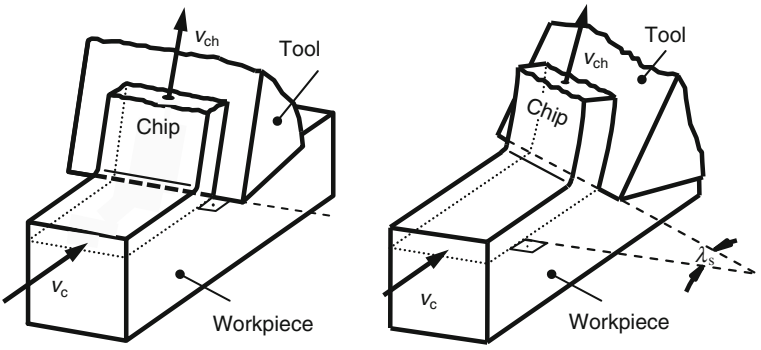

Fig. 3.9 Free, orthogonal and free, diagonal cut

The free, orthogonal cut is a special case, which can be brought about by the following marginal conditions:

- Only the major cutting edge is being engaged (free).
- The tool cutting edge angle κ_r is 90° (orthogonal).
- Tool cutting edge inclination λ_s is equal to 0° (orthogonal).

Practically speaking, this cut can be executed, for example, by means of longitudinal face turning or cross cylindrical turning (see Sect. 9.1) allowing for the above marginal conditions (Fig. 3.9).

The free, diagonal cut is more general and contains the free, orthogonal cut. The following marginal conditions must be realized in the case of the free, diagonal cut:

- Only the major cutting edge is engaged (free).
- The tool cutting edge angle κ_r can take on values that are not equal to 90° (diagonal).
- Arbitrary tool cutting edge inclinations λ_s are permissible (diagonal).

As soon as one of the last two marginal conditions is fulfilled, it is a free, diagonal cut. Both conditions don't have to be met simultaneously, although this can occur.

The general case, the bound, diagonal cut (Fig. 3.10), contains all abovementioned special cases and, in addition to the marginal conditions of the free, diagonal cut, also permits the engagement of the minor cutting edge (bound).

All the basic process variants can be further extended by adding the following categories:

- The uninterrupted cut and
- the interrupted cut.

The interrupted cut is the general variant among them, in which the cut takes place only intermittently. In the case of the uninterrupted cut, temporal interruption is infinitely small (the cut is continuous). Both process possibilities will be described

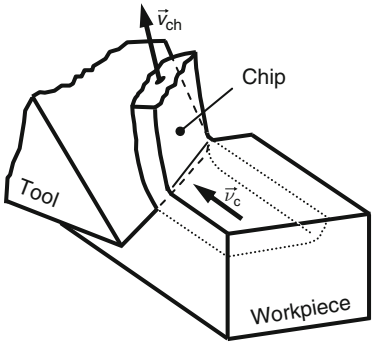

Fig. 3.10 Bound diagonal cut

in great detail in later chapters (see Chaps. 9 and 10). In total, there are therefore six basic process variants.

3.4 Chip Formation

At the beginning of the chip formation process, the cutting section penetrates the material, causing it to deform elastically and plastically. After the maximum permissible material-dependent shear stress is exceeded, the material begins to flow. Contingent on a given cutting section geometry, the deformed material forms a chip, which runs off the rake face of the cutting section.

The property of plastic deformability is not solely related to the material; it can also be brought about in a targeted way by altering the stress. The amount of stresses is influenced by the feed velocity v_f, the cutting speed v_c and the depth of cut a_p. As far as process kinematics is concerned, the direction of cutting section stress is determined by defining the tool normal rake angle γ_n, the tool cutting edge angle κ_r and tool cutting edge inclination λ_s.

In order to ensure chip formation, a minimum chip thickness and depth of cut must be exceeded (see Chap. 7 [Moll39, Djat52, Soko55, Bram61, Bram60]).

3.4.1 The Cutting Process

By varying the direction and amount of stress, either tough or brittle material behaviour can be realized [Karm11, Böke14]. This has a large effect on chip formation. During cutting, the direction of a particular stress can be set by the process parameters tool normal rake angle, tool cutting edge angle and tool cutting edge inclination. The amount of the particular stress is influenced by the cutting parameters cutting speed, feed velocity and depth of cut. To put it another way, the same material can be tough or brittle depending on the direction and amount of stress,

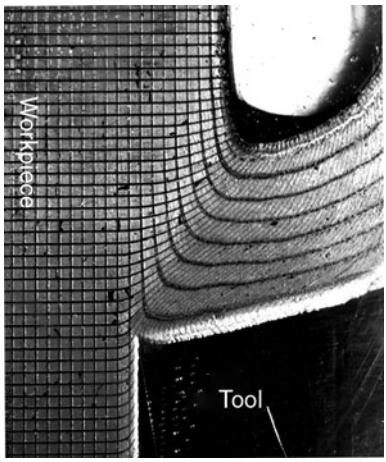

Fig. 3.11 Model representation of deformation, acc. to Leopold [Leop00]

independently of how it behaves at room temperature and under single-axis tensile loads (tension test).

When cutting steel, one must bear in mind that brittle behaviour only occurs at very low temperatures. This is not the case when machining cast iron, glass and ceramics. There is brittle fracture behaviour for these materials even at high temperatures due to their material structures. The particular stress must therefore be optimally adjusted to the given material properties with process kinematics in both direction and amount.

To clarify plastomechanical processes during chip formation, a grid is superimposed on the workpiece (Fig. 3.11) so that material deformation during cutting can be observed (the visioplasticiy method) [Hast67, Chil71, Leop80, Leop00]. With this method, the chip formation process can be made visible, and with the help of this, chip formation models can be made. Finite element analysis is another possibility for modelling chip formation. The visioplasticity method can help to verify FE modellings, since it allows for a temporal and local definition of chip formation on the superimposed grid [Leop80].

Special marginal conditions exist during chip formation: both high rake face temperatures (about 770–1700°C) as well as high deformation speeds (of an order of magnitude of 10^4/s).

Figure 3.12 is a schematic representation of the chip formation process as sketched with the help of a photograph of chip initiation (right).

In this representation, we can see a continuous plastic deformation that can be subdivided into four zones. The transition from the workpiece structure (a) to the chip structure (b) is made by simple shearing (shear zone). When cutting brittle materials, minor deformation on the shear plane can already lead to material detachment.

If however the material has higher deformability, detachment first occurs in front of the cutting edge in zone (e). The tensile load under simultaneous perpendicularly

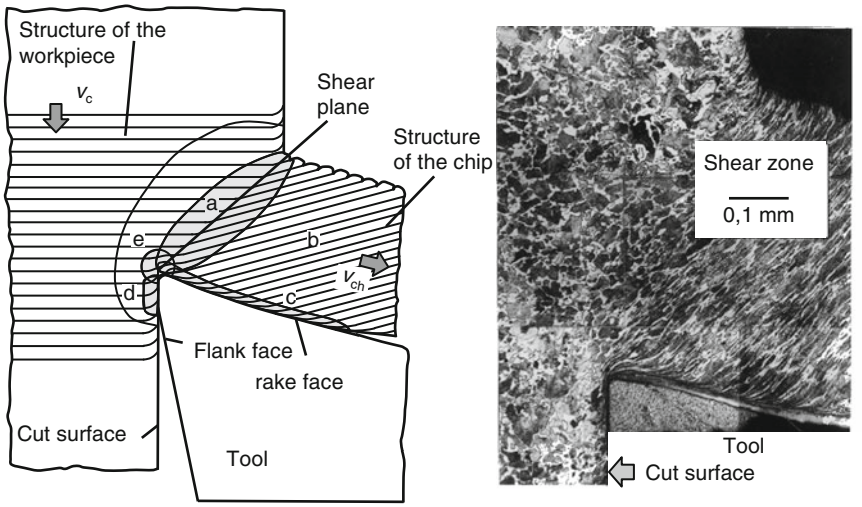

Fig. 3.12 Location of chip initiation

active pressure leads, together with the high temperatures prevalent here, to strong deformations on the peripheries of the rake face (c) and cut surface (d). Sliding over the tool surfaces causes further plastic deformations to arise in the boundary layers. The "flow zone" (the non-etched white zone on the bottom of the chip), the deformation texture of which forms parallel to the rake face, gives the impression of a viscous flow process with an extremely high degree of deformation. The chip resulting from the described chip formation process is designated as a continuous chip. Other chip types include lamellar chips, segmented chips and discontinuous chips.

Figure 3.13 shows a quantitative profile of normal and tangential stresses resulting from the resultant force components acting on the rake face. These stresses – in conjunction with temperatures prevalent in the contact zone, which can amount to over 1000°C in the continuous chip formation zone – lead to deformations with sheer strains $\bar{\varepsilon}$ between 0.8 and 4.0 and sheer strain speeds $\dot{\bar{\varepsilon}}$ of up to 10^6/s. For the sake of comparison, Fig. 3.13 provides corresponding figures from the tension test. Cutting conditions under which cemented carbide tools operate result in deformation and material heating durations in the order of magnitude of milliseconds; the heating velocities are theoretically around 10^6°C/s [Opit70].

3.4.2 Different Types of Chip Formation

When chip formation has been ensured, it can occur in different ways. ERNST [Erns38, Erns41] has made a phenomenological classification of chip formation types. Continuous chip formation is characterized by an evenly deformed material

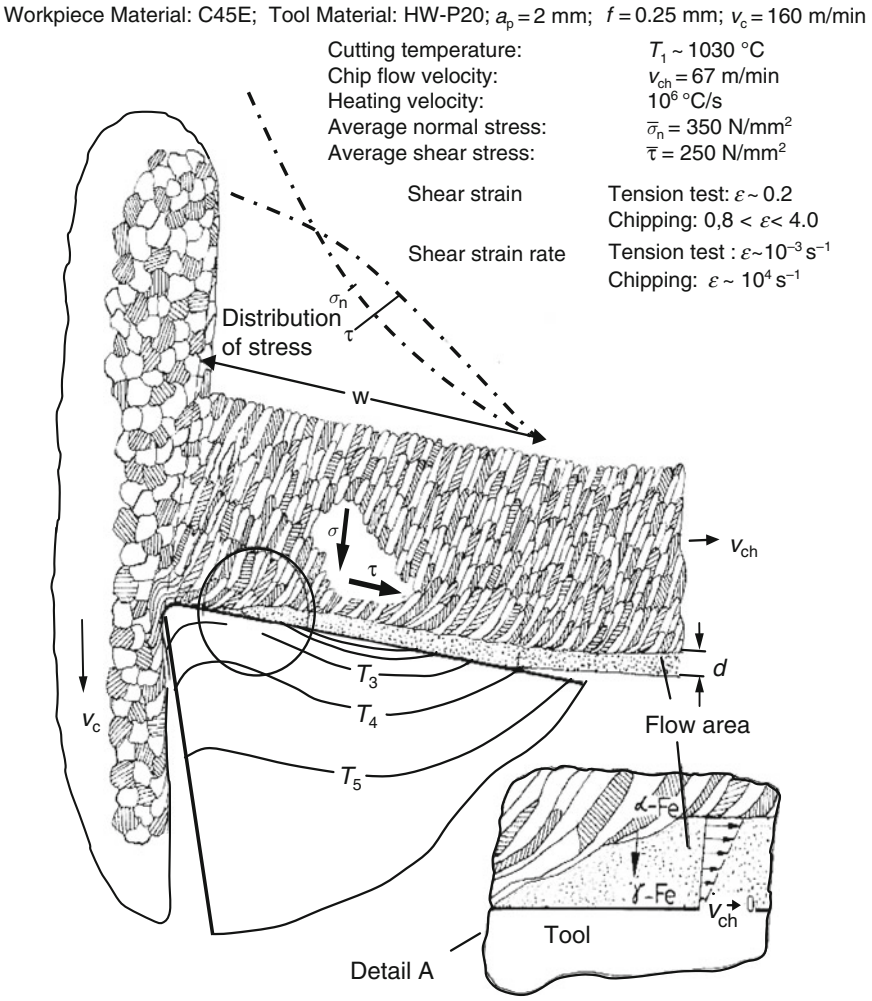

Fig. 3.13 Conditions of the cutting process, acc. to KÖNIG [Köni67]

chip structure, the cause of which is assumed to be in the temporally highly uniform friction conditions between the chip and the tool.

Lamellar chip formation is characterized by an unevenly deformed material structure between the chip and the tool, the cause of which is explained by temporally highly altered friction conditions between the chip and the tool (stick-slip) or by dynamic stress transfer [Scha64]. Locally enhanced structural deformations, shear bands, can be recognized in the chip structure, that are characteristic of this type of chip formation.

The frequencies of the vibrations caused by stick-slip are in the range of kilohertz and have small amplitudes. The high level of local structural deformation is

explained by the fact that the thermally caused material softening is more dominant than its mechanical hardening. Research into these phenomena relies on the work of ZENER and HOLLOMON, who have described them and conceived the term "shear band". Shear bands appear when machining high-strength materials with high levels of deformability. They are also especially frequent when machining with high cutting speeds [Hopp03].

If the stress condition in the shear zone exceeds the deformability of the material (shear strength), there is a detachment of material areas, which then fuse with each other again. This leads to the formation of segmented chips. This can be conceived of as a special case of lamellar chip formation in which highly localized deformations (shear bands) arise as well.

In addition to vibrations, the entire system – consisting of the machine tool, tool, workpiece and fixtures – is influenced by further dynamic effects such as the regenenerative effect or directional coupling [Weck77]. The frequencies of these effects are much lower, in the area of a thousand hertz. In contrast to the higher-frequency chip formation dynamics, these vibrations do not so much influence chip formation in the sense of material deformation as much as chip formation from outside, since they are the cause of dynamic alterations in the nominal feed.

SCHWERD has made microcinematographic experiments and suggested the concept of "discontinuous chip" [Schw36]. This process basically distinguishes itself from the other processes of chip formation by the fact that no plastic deformation occurs before fracture, but rather fracture takes place without plastic deformation. Discontinuous chips can be observed in the case of materials with very brittle properties, e.g. cast iron, stone, fibre-reinforced plastic or titanium alumnides.

Figure 3.14 summarizes the principal chip types [Vier70].

- Continuous chips form when the material has sufficient deformability ($\varepsilon_B > \varepsilon_0$), the microstructure is uniform in the cutting area, deformation does not cause embrittlement and chip formation is not impaired by vibrations.
- Lamellar chips form when $\varepsilon_B < \varepsilon_0 < \varepsilon_F$ or the microstructure is not uniform or vibrations lead to variations in chip thickness. Lamellar chips can form with high feeds as well as with high cutting speeds.
- Segmented chips consist of chip segments that are separated in the shear plane and fuse together again. The form when $\varepsilon_F < \varepsilon_0$, whereby this is not only the case for brittle materials like cast iron but also can come about if deformation causes embrittlement in the microstructure. Segmented chips can also be formed at extremely low cutting speeds ($v_c = 1 - 3\,\mathrm{m/min}$).
- Discontinuous chips most form when cutting brittle materials with uneven microstructures such as certain types of cast iron and stone. The chips are not detached, but are torn off the surface, often causing damage due to small breakings from the workpiece surface.

Figure 3.15 gives a tool-oriented overview of the dynamic system of spheres of influence, all complexly overlapping and mutually retroactive, which brings about

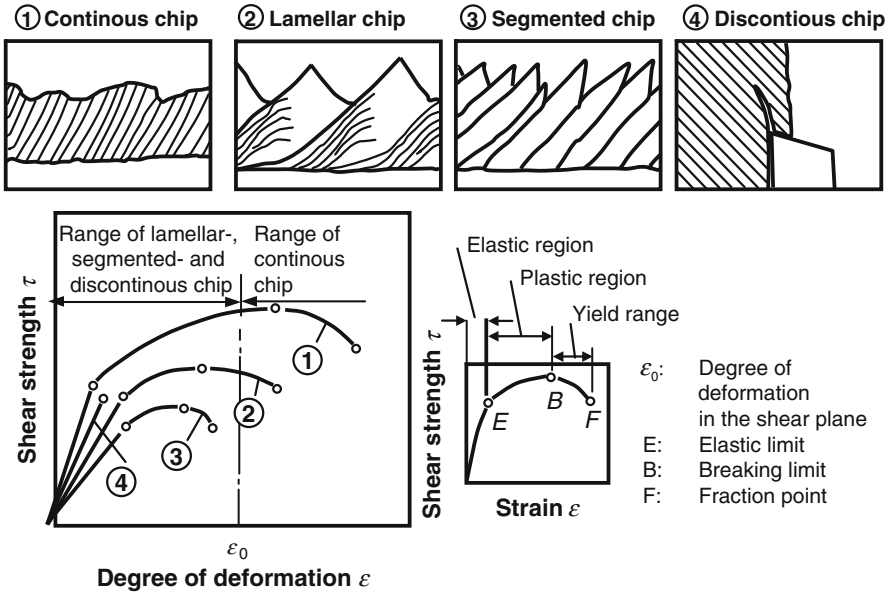

Fig. 3.14 Types of chip depending on material properties, acc. to VIEREGGE [Vier70]

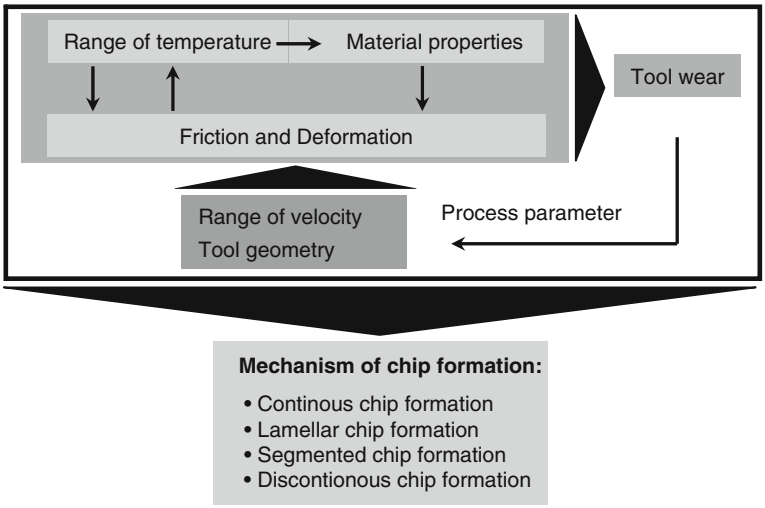

Fig. 3.15 Influence on chip formation

the various types of chip formation. This system is heavily influenced by the velocity fields, the materials to be machined, tool geometry and process kinematics.

This section will not deal with low-frequency dynamic effects on the part of the machine tool. See the relevant literature for further information [Kron54, Opit70, Weck77, Alti00].

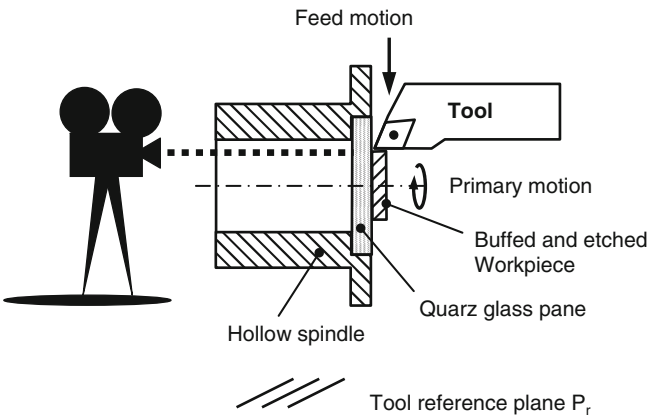

Fig. 3.16 Microcinematograpy

One method with which chip formation is directly observable, is microcinematography, the first application of which on the cutting process was already carried out by KURREIN and then later by KLOPSTOCK [Kurr05, Klop23, Klop26] (see Fig. 3.16).

The development of this process has been advanced by several researchers in the course of time [Schw36, Merc45, Oxle59, Spaa71, Warn74]. In this process, chip formation is observed through a quartz glass pane while photos are taken or films are recorded successively in short intervals. One disadvantage of this procedure is the limitation to very low cutting speeds ($v_c = 1$ cm/min). Nevertheless, the process has helped to explicate basic phenomena.

Today there are high-speed cameras available that can capture 150,000 images per second. With such cameras, the phenomena can be made visible at the lower threshold at higher speeds or especially during micro-cutting.

In order to be able to study chip formation more effectively, various methods have been developed for cut interruption. During the cutting process, chip roots are held "in statu nascendi", providing information about chip formation after subsequent metallographic preparation. In the case of the equipment used today, the tool is suddenly accelerated out of the cut. The acceleration is brought about by a predetermined breaking point on the swivel device that breaks during the cutting process due to an impulse caused by an explosion [Lola49] (Fig. 3.17). Gente has recently developed a method in which the delay time and the masses moved can be reduced in comparison with the "explosion method" [Gent02] (see also Fig. 3.17). In this way, investigations into chip roots are also possible with higher cutting speeds.

Other methods have been developed in which a chip root is produced in the workpiece by means of a predetermined breaking point (brittle fracture, Fig. 3.18) [Buda68]. The advantage is that that chip root is detached from the workpiece so that the effective area can be spared during the following metallographic preparation.

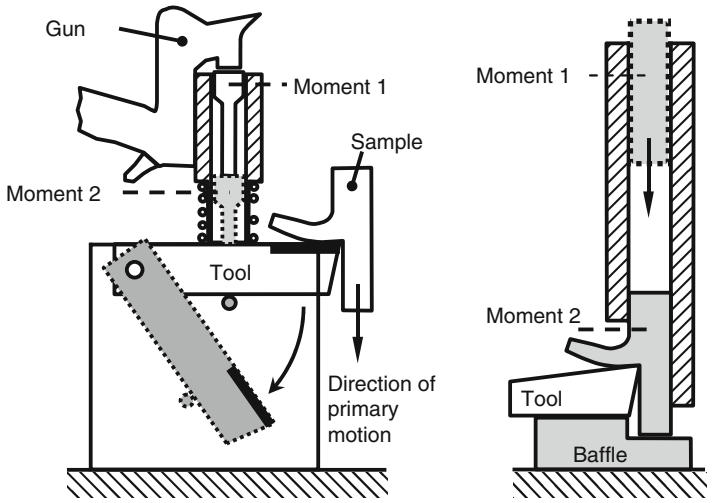

Fig. 3.17 Interruption of cutting process, acc. to LOLADSE [Lola49] (*left*) and GENTE [Gent02] (*right*)

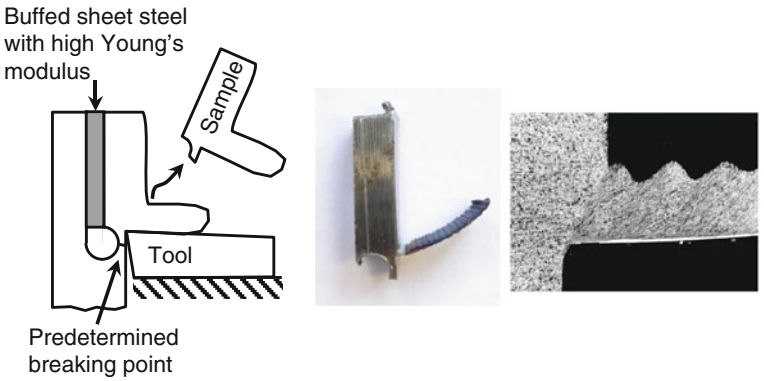

Fig. 3.18 Interruption of cutting process by predetermined breaking point, acc. to BUDA [Buda68]

3.5 Kinematic Surface Roughness

Calculations of interpenetration between the tool and the workpiece can provide key information about the cutting process, including the associated undeformed chip cross-sections in the case of changing engagement parameters (see also gear manufacture) or micro-geometrical surface parameters. The following shows by way of example the generation of surface quality for a simple external turning process. Since chip formation processes are ignored, we speak in this case of the generation of kinematic surface roughness. For this, the penetration of the workpiece by the tool is geometrically evaluated taking into consideration the kinematics in the tool reference plane P_r (Fig. 3.19).

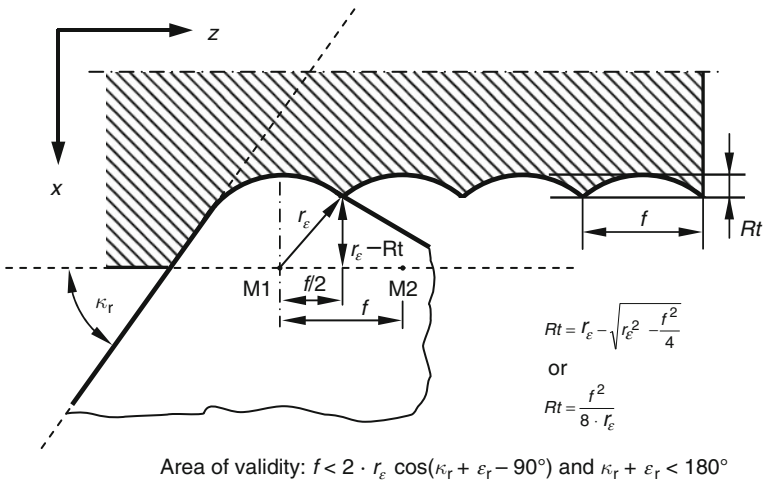

Fig. 3.19 Geometric ratio of engagement in the cutting process

3.6 Mechanical and Thermal Strain on the Cutting Section

The resultant force F, represented here in the turning process as an example, can be decomposed into the components cutting force F_c, feed force F_f and passive force F_p (Fig. 3.20). Currently, these resultant force components are usually detected metrologically with the help of piezoelectric force sensors.

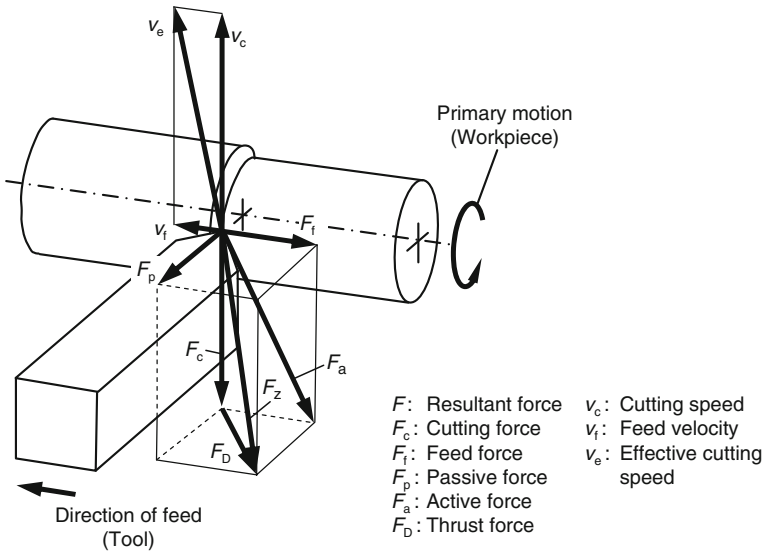

Fig. 3.20 Resultant force and its components in the cutting process, acc. to DIN 6584

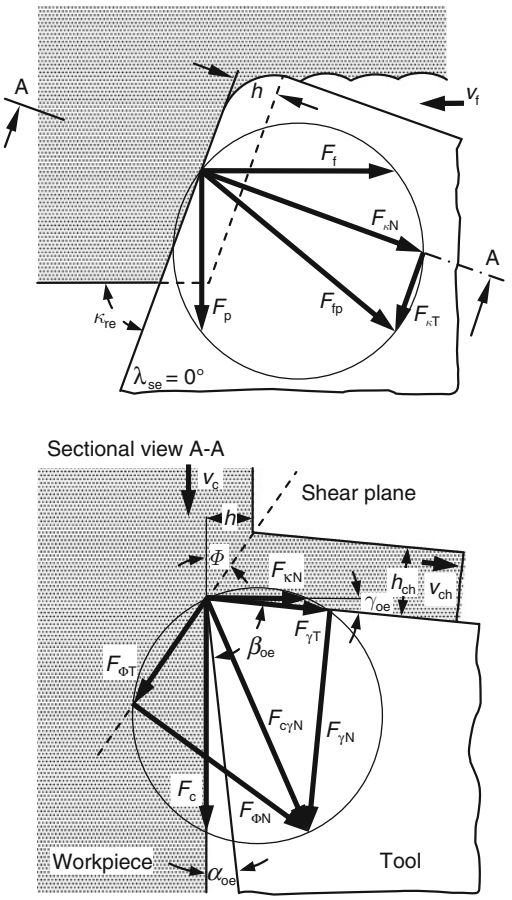

F_c	Cutting force
F_f	Feed force
F_p	Passive force
F_{fp}	Resultant of F_f and F_p
$F_{\kappa N}$	Normal force of major cutting edge
$F_{\kappa T}$	Tangential force of major cutting edge
$F_{\gamma N}$	Normal force of rake face
$F_{\gamma T}$	Tangential force of rake face
$F_{\Phi N}$	Normal force of shear plane
$F_{\Phi T}$	Tangential force of shear plane
$F_{c\gamma N}$	Resultant of $F_{\gamma T}$ and $F_{\gamma N}$, or $F_{\Phi T}$ and $F_{\Phi N}$
h	Undeformed chip thickness
h_{ch}	Chip thickness
v_c	Cutting speed
v_{ch}	Chip speed
α_{oe}	Tool orthogonal clearance
β_{oe}	Wedge angle
γ_{oe}	Tool orthogonal rake angle
κ_{re}	Working cutting edge angle
λ_{se}	Working cutting edge inclination
Φ	Shear angle

Fig. 3.21 Components of resultant force in working plane of reference (*top*) and working plane (*below*)

The analysis of forces derived for the orthogonal cut by Merchant [Merc45, Merc45a] is the basis for determining the forces acting on the tool cutting edge (Fig. 3.21).

Assuming an ideally sharp cutting edge and neglecting flank face wear, the tangential force $F_{\gamma T}$ and the normal force $F_{\gamma N}$ acting on the tool can be calculated from the force components. The following applies as long as the inclination is $\lambda_s = 0°$ and the influence of the minor cutting edge is slight:

$$F_{\gamma N} = F_c \cos \gamma_o - (F_f \sin \kappa_r + F_p \cos \kappa_r) \sin \gamma_o \tag{3.1}$$

$$F_{\gamma T} = F_c \sin \gamma_o + (F_f \sin \kappa_r + F_p \cos \kappa_r) \cos \gamma_o \tag{3.2}$$

where the bracket term in Eqs. (3.1) and (3.2) corresponds to the normal force of the major cutting edge $F_{\kappa N}$ (Fig. 3.21). Because of the (in most cases) small difference between the angles in the tool-in-hand system and the tool-in-use system, calculations are made within the tool-in-hand system for the sake of simplicity.

For the case $\gamma_o = 0°$, the cutting force F_c and the feed force F_f act perpendicularly/tangentially to the rake face. In contrast to Merchant's original work, a neutral tool orthogonal rake angle ($\gamma_o = 0°$) was selected, and the forces were shown with the effective cutting direction on the tool cutting edge. Designation of the acting forces and their signs is derived from the standards ISO 3002/4 and DIN 6584.

As Fig. 3.22 clarifies for the simplest case of an orthogonal cross section with a neutral tool orthogonal rake angle, the cutting and feed forces on the worn tool are composed not only of the normal force of the rake face $F_{\gamma N}$ and the tangential force of the rake face $F_{\gamma T}$ but also of the tangential force of the flank face $F_{\alpha T}$ and the normal force of the flank face $F_{\alpha N}$. The friction coefficient, which can be calculated from the cut and feed forces, thus contains not only rake angle friction but also forces acting on the flank face caused for example by elastic deformation of the workpiece surface and by tool wear [Klau65]. As research has shown, the normal force of the flank face amounts to about 40% of the feed force and thus to

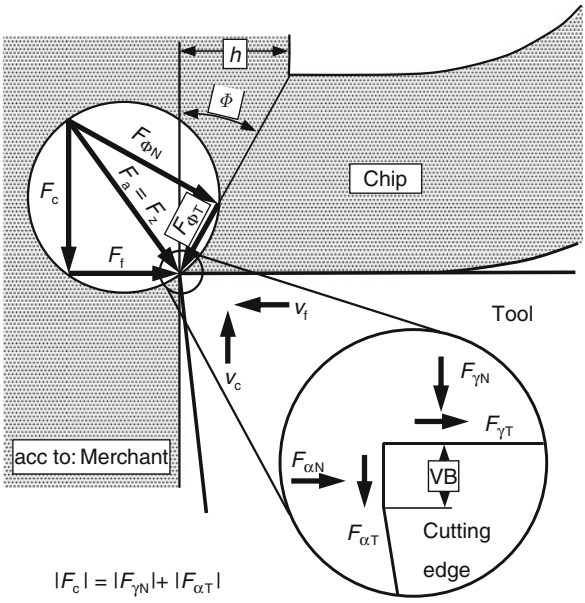

Fig. 3.22 In the cutting process the mechanical strain of the cutting edge results from normal and tangential forces and their components acting on rake and flank face, acc. to MERCHANT [Merc45, Merc45a]

about 66% of the rake face component in the feed direction [Spaa67, Lutz68]. A percentage of approximately 10% of the cutting force F_c was ascertained for the tangential force of the flank face.

The average normal and tangential stresses originating from the resultant force components acting on the rake face are between 350 and 400 N/mm^2 or between 250 and 350 N/mm^2 when machining construction steel [Köni72].

Materials that are difficult to cut result in values of 1100 N/mm^2. Their profile is qualitatively reproduced in Fig. 3.13. The size and direction of the resultant force are strongly influenced by the cutting parameters and cutting section geometries used. Figure 3.23 shows the dependence of the static components of the resultant cutting force F_c, F_f and F_p on the feed f, cutting speed v_c, depth of cut a_p and the tool cutting edge angle κ_r qualitatively in a linear coordinate system.

The extremes in the profiles of the resultant force components over cutting speed can be ascribed to growth of built up-edge. The reduction of forces with increasing cutting speed is caused by the reduction of material strength at higher temperatures. The components of the resultant force increase proportionally over the depth of cut a_p. Yet this is only valid if the depth of cut is larger than the corner radius of the tool. The profile of feed force F_f and passive force F_p over the tool cutting edge angle κ_r results from the geometric position of the cutting edge with respect to the workpiece axis, since with a larger cutting edge angle the resultant force component aimed in the feed direction increases, and its maximum is reached at $\kappa_r = 90°$. If the tool cutting edge angle is increased, the undeformed chip thickness h increases proportionally to the reduction of the width of undeformed chip b. Since cutting

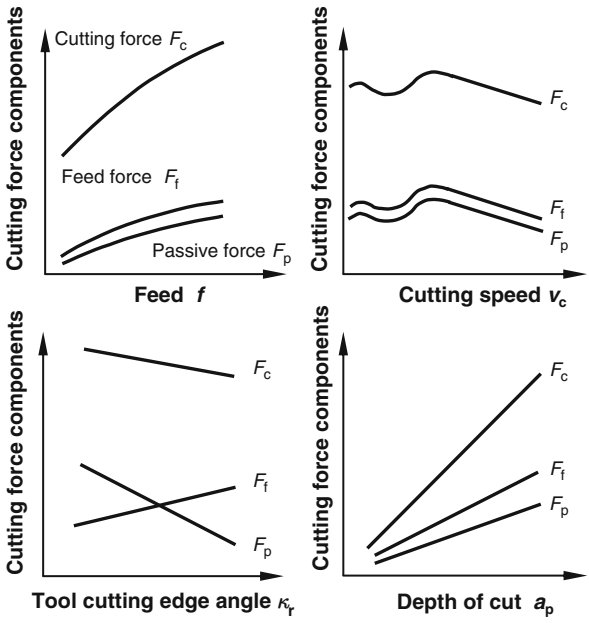

Fig. 3.23 Components of resultant force depending on feed, cutting velocity, tool cutting edge angle, and depth of cut (qualitative)

Influencing variables		Change of cutting force components per degree angle variation		
		Cutting force F_c	Feed force F_f	passive force F_p
Decreasing	Tool orthogonal rake angle	⇧ 1.5 %	⇧ 5.0 %	⇧ 4.0 %
	Tool cutting edge inclination	⇧ 1.5 %	⇧ 1.5 %	⇧ 10.0 %
Increasing	Tool orthogonal rake angle	⇩ 1.5 %	⇩ 5.0 %	⇩ 4.0 %
	Tool cutting edge inclination	⇩ 1.5 %	⇩ 1.5 %	⇩ 10.0 %

Fig. 3.24 Influence of cutting edge and rake angle on the components of the resultant force

force F_c is proportional over depth of cut a_p($\hat{=}$ width of undeformed chip b) but increases degressively over feed ($\hat{=}$ undeformed chip thickness h), a light reduction of F_c with increasing κ_r is the outcome of both changes.

Figure 3.24 provides some standard values for how the components of the resultant force change if the tool orthogonal rake angle or the cutting edge inclination is varied. This information can vary greatly however and should only be seen as reference values.

Changing the tool orthogonal clearance angle in the range of $3 \leq \alpha_o \leq 12°$ has no mentionable effects on the resultant force components. Changing the corner radius also does not have a significant effect on the forces as long as the condition $2r \leq a_p$ is met.

Tool wear (see Sect. 3.7) is another variable that influences resultant forces. Varying effects on the components of the resultant force can be observed depending on the type of wear.

Crater wear, resulting in a larger positive tool orthogonal rake angle, generally leads of a reduction of cutting forces. On the other hand, these forces increase when flank face wear is dominant since the friction surface between the workpiece and the flank face becomes larger. Quantitative determinations concerning force increase with increasing tool wear can only be approximated due to the large number of influencing parameters. The following reference values can be assumed approximately for force increase up to a width of flank wear land of VB = 0.5 mm: About 90% for the feed force F_f, about 100% for the passive force F_p and about 20% for the cutting force F_c.

Several specific characteristic values can be distinguished for calculating the components of the resultant force. These component forces are directly proportional to the width of undeformed chip b. To identify empirical laws, it is usually advisable to relate the measurement to already known, linearly dependent magnitudes in

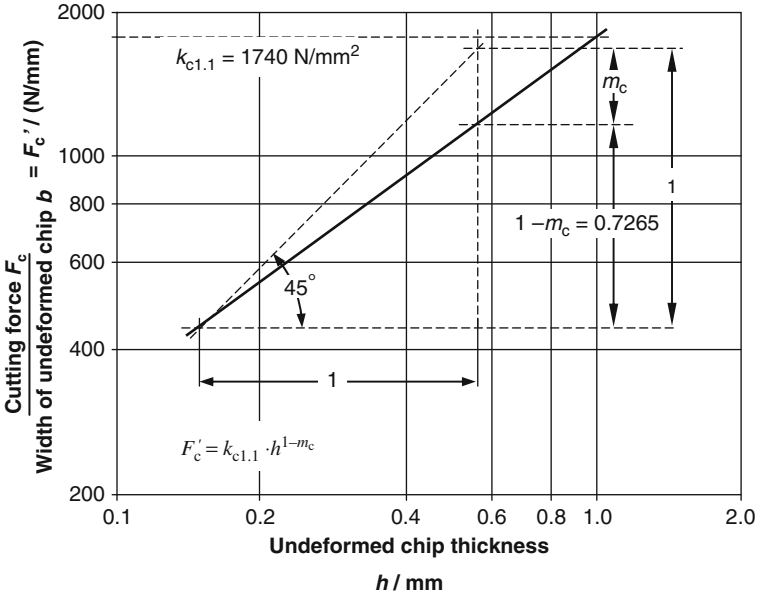

Fig. 3.25 Graphical determination of characteristic values $k_{c1.1}$ and $(1–m_c)$

order to minimize the number of variables going into the physical law. In this case, we form the quotient F_c' from the cutting force F_c and the width of undeformed chip b. If we now plot the values thus found over undeformed chip thickness h in a double logarithmic plot, the measurement points arrange themselves in a straight line (Fig. 3.25).

The corresponding linear equation

$$\log(F_c/b) = \log(k_{c1.1}) + (1 - m_c) \cdot \log h \tag{3.3}$$

can be converted into the KIENZLE Equation

$$F_c' = k_{c1.1} \cdot h^{(1-m_c)} \tag{3.4}$$

The specific cutting force $k_{c1.1}$ is the cutting force required to detach a chip of undeformed chip width $b = 1$ mm and undeformed chip thickness $h = 1$ mm. The exponent $(1–m_c)$ designates the gradient of the straight line $F_c' = f(h)$ in the double logarithmic system.

To determine $k_{c1.1}$ and $(1–m_c)$, cutting experiments are carried out for the combination of workpiece material and cutting tool material under investigation. In these experiments, the relevant cutting forces are measured with constant cutting speed, depth of cut and cutting section geometry and plotted in accordance with Fig. 3.25. The required specific cutting force characteristic parameter $k_{c1.1}$ is determined by

extrapolating the undeformed chip thickness to $h = 1$ mm. The tangent of the angle between the straight line and the x-axis is the desired gradient value $(1–m_c)$.

Corresponding equations and characteristic values can be defined for resultant force components F_f and F_p:

$$F_f^{'} = k_{f1.1} \cdot h^{(1-m_f)} \tag{3.5}$$

$$F_p{}' = k_{p1.1} \cdot h^{(1-m_p)} \tag{3.6}$$

The values determined in this way are however only valid for undeformed chip thicknesses of $h > 0.1$ mm. Values for k_c and $(1–m)$ can be found in [Köni82].

According to DIN 6584, the energy for cutting is the result of the product of the paths to be travelled or paths travelled and the components of the resultant force acting in their direction. Correspondingly the powers arising during the cutting process result from the product of the speed components and the components of the result force acting in their direction.

Cutting energy W_c and cutting power P_c:

$$W_c = l_c \cdot F_c \tag{3.7}$$

$$P_c = v_c \cdot F_c \tag{3.8}$$

Feed energy W_f and feed power P_f:

$$W_f = l_f \cdot F_f \tag{3.9}$$

$$P_f = v_f \cdot F_f \tag{3.10}$$

Effective energy W_e and effective power P_e are understood as the sum of all corresponding cut and feed amounts:

$$W_e = W_c + W_f \tag{3.11}$$

$$P_e = P_c + P_f \tag{3.12}$$

Due to the relatively low feed speeds and feed paths, feed energy/power during turning amounts to only about 0.03–3% of the corresponding cutting energy or cutting power. For this reason, we can assume $W_e \approx W_c$ and $P_e \approx P_c$ for most cases.

Figure 3.26 provides an overview of the segmentation of the total active energy into shear, cutting and friction energy as a function of the undeformed chip thickness [Vier70]. The illustration shows that the amounts of the different types of energy depend on the undeformed chip thickness, whereby shear energy has the largest share for most undeformed chip thicknesses.

The mechanical work used in cutting is almost completely converted into thermal energy. Since the heat centres are identical with the deformation centres, the shear

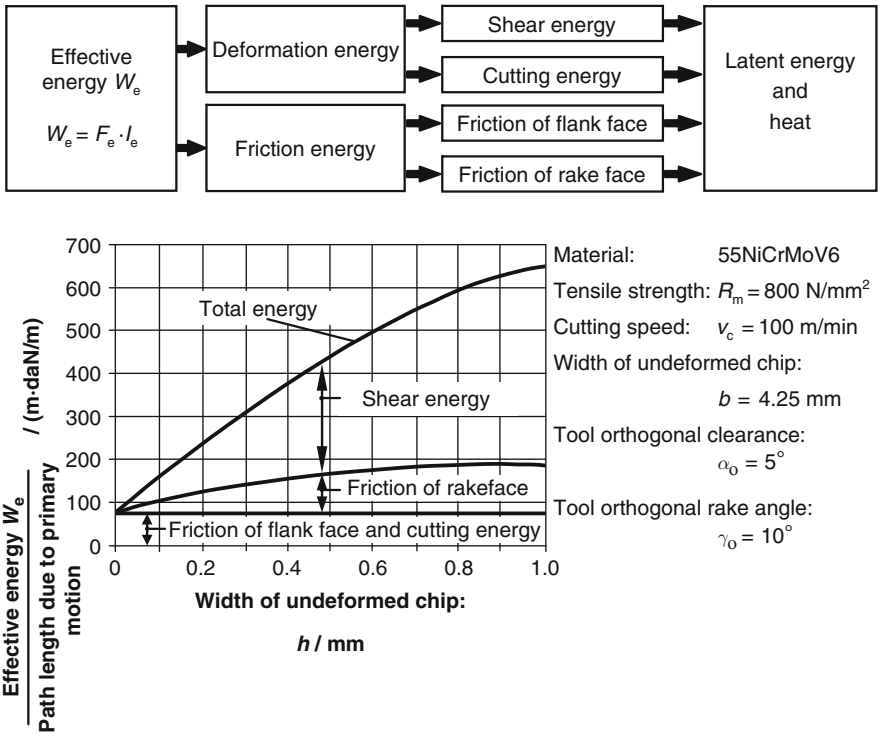

Fig. 3.26 Segmentation of effective energy in cutting process depending on chip thickness, acc. to VIEREGGE [Vier59, Vier70]

zone and the friction zones on the tool come into consideration as heat sources. As Fig. 3.13 shows, the degree of deformation on the bottom of the chip is much higher in the flow zone than in the shear zone, so one can expect the highest temperatures between the chip and the tool. Since the thickness of the flow zone is very small in comparison with the shear zone however, these higher temperatures should not also be equated with a high energy conversion.

The illustration in Fig. 3.27 left gives information about heat that is absorbed/dissipated by the workpiece, chip and tool. Most of the heat is dissipated by the chip. Most of the mechanical energy (in this case 75% and generally more than 50%) is converted in the shear zone. The heat arising in the individual development locations is dissipated by thermal conduction, radiation and convection to the environment. As a result of this heat balance, corresponding temperature fields form in the workpiece and tool that change until equilibrium between added and removed heat is achieved. The right side of the figure shows such a temperature field.

If we consider one material particle in the cutting zone, its temperautre will be at least equal to that of a particle in the shear zone. As it glides further into the contact zone, the material is intensively heated on the chip bottom side and the tool on the rake face, because the energy required to overcome friction between the chip

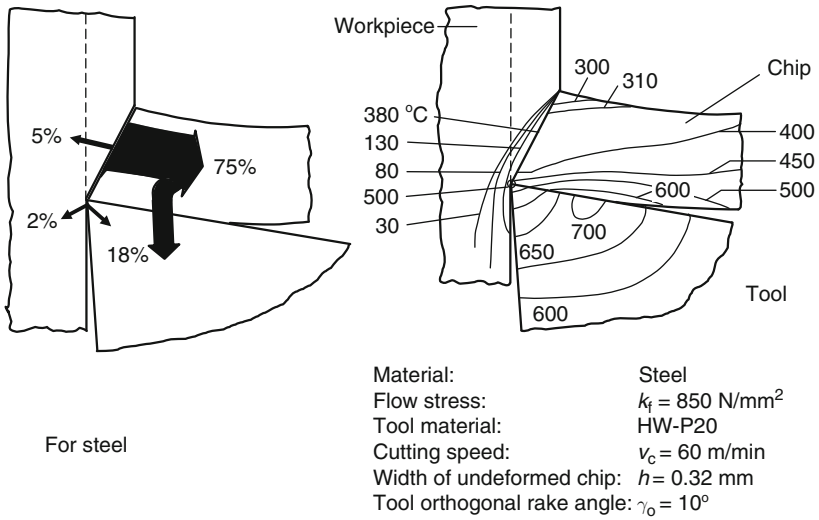

Fig. 3.27 Distribution of heat and temperature in workpiece, chip, and tool in the process of steel cutting, acc. to KRONENBERG [Kron54] and VIEREGGE [Vier59]

and the rake face is almost completely converted into heat. Since this process only takes place in boundary layers of the chip and cutting tool material it heats up the rake and chip bottom side all the more strongly the less time is available for heat dissipation due to the higher cutting speeds. The maximum temperature does not appear directly on the cutting edge, but rather at a certain distance from it on the rake face depending on the cutting conditions.

Determining the temperatures arising during cutting has long been the subject of intensive research [Gott25, Lang49, Schm53, Küst54, Vier55, Küst56, Axer55]. Already in 1956, KÜSTERS demonstrated temperatures of over 1000°C on the rake face when cutting steel with cemented carbide [Küst56]. Later investigations have qualitatively confirmed these results again and again [Cass94, Denk90, Ehme70a, Lenz66, Laus88, Beye72, Dama90, LoCa94]. The level of the temperatures acting on the cutting section depends on the machined material, the cutting tool material, the selected cutting conditions, tool wear and the cooling medium. Figure 3.28 provides an impression of the order of magnitude of the mean cutting temperatures to be expected on the rake face as a function of cutting speed for various cutting tool materials. In the v_c = 20–50 m/min range, the temperature profile is non-linear in the double logarithmic coordinate system. The reason for this is the the growth of built up-edge arising in this cutting speed range (see Sect. 3.7.2), which interferes with direct heat conduction.

In comparison to the rake face, temperatures on the flank face are generally low (Fig. 3.29) [Denk90, Ehme70a, Axer55, Laus88, Beye72, Dama90]. The size of the temperature difference between the rake face and the flank face, about 200–300°C

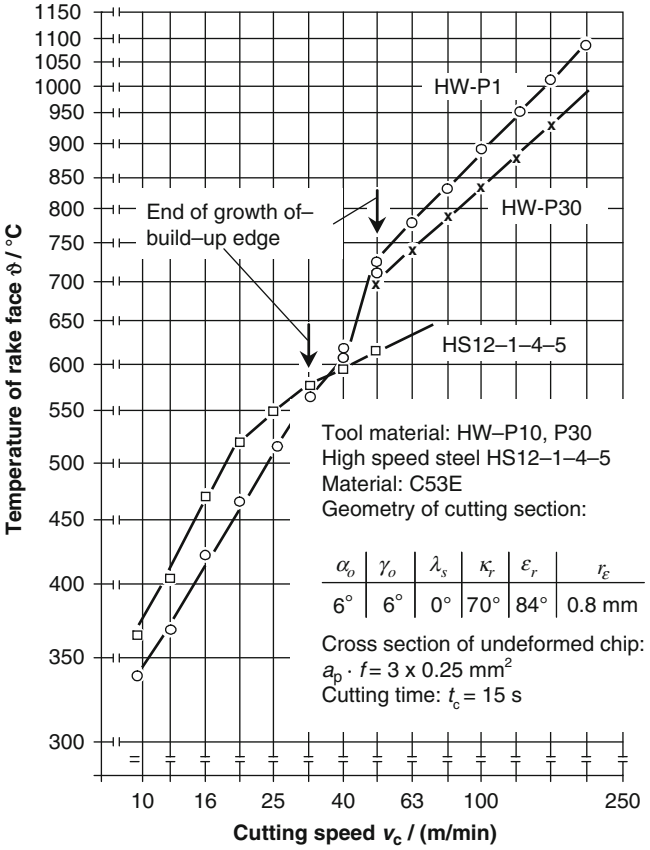

Fig. 3.28 Mean rake face temperature

when cutting with cemented carbide tools according to [Ehme70a], is strongly co-determined by the position of the contact zone on the rake face. The closer the rake face moves towards the cutting edge, the more the temperatures prevalent on the rake and flank faces conform. This means that temperatures are very high on the flank face as well, especially during finishing operations with high cutting speeds and small feeds. According to the information provided by the literature [Ehme70a, Vier53, Schm53, Küst54, Vier55, Küst56, Axer55, Beye72], temperatures of over 800°C can be found on the flank face depending on the selected marginal conditions when cutting with cemented carbide tools.

There are various methods and devices available for temperature measurement during the cutting process (Fig. 3.30) [Lowa67], which vary according to technique, experimental setup and measurement position. The only metrological techniques that come into question for measuring temperature during the cutting process are time-resolution measurement techniques, since the cutting process duration (and thus the achievement of a thermally stationary state) is too short for other methods

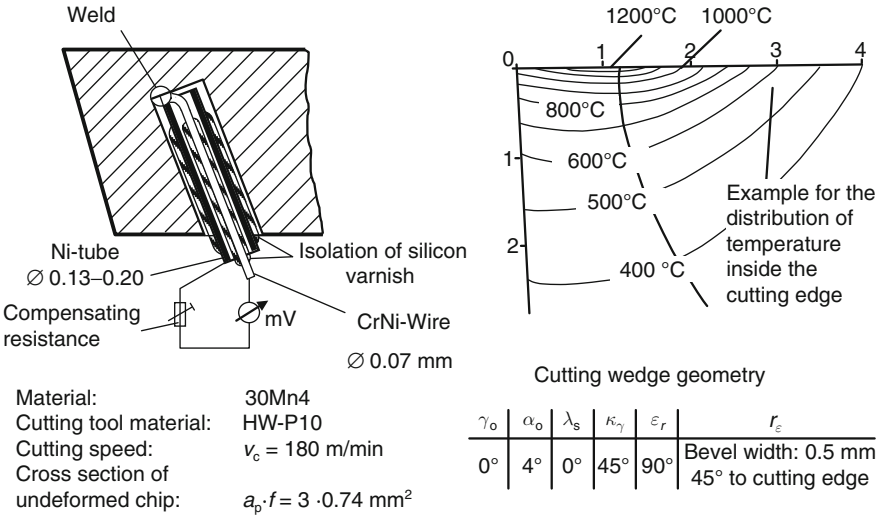

Fig. 3.29 Measurement of temperature with embedded thermocouple on cemented carbide, acc. to Küsters [Küst56]

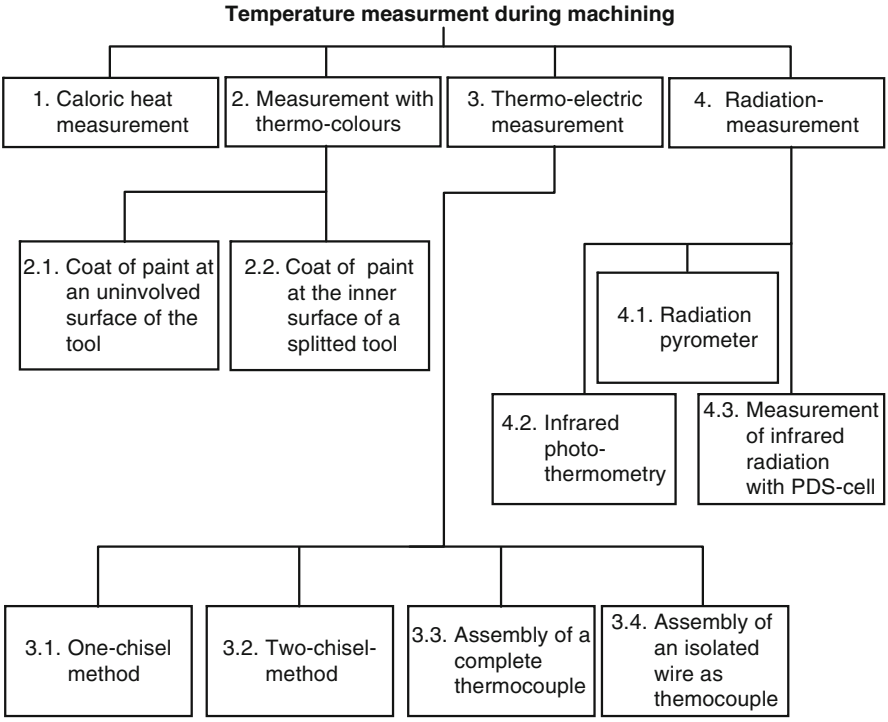

Fig. 3.30 Temperature measurement in cutting processes

(e.g. coating with temperature-sensitive colours or powders with constant melting points). Of the processes introduced in Fig. 3.30, the one and two-chisel methods, temperature measurement with thermocouples, pyrometers and photo thermometry are of technical interest.

GOTTWEIN developed the one-chisel method as the first direct method for measuring temperature and then, in cooperation with REICHEL, the two-chisel method [Gott25, Herb26, Vier70]. Both methods are based upon the principle of a thermocouple. Both tool and workpiece form the heat soldering joints, while the tool clamp is the cold soldering joint. The workpiece and the tool must be clamped in isolation, since the thermoelectric voltage arising in the contact zone between the cutting insert and the chip would otherwise be dismantled through the machine in a short circuit. Contact between the passing chip and the workpiece outside of the contact zone must therefore also be avoided. Both methods require electrically conductive materials and cutting tool materials. In the case of the two-chisel method, cutting tool materials with varying thermoelectric properties must be used. The greatest disadvantage of the single-chisel method is the protracted and elaborate process needed to calibrate the thermocouple which must be carried out again for every cutting tool material and workpiece material combination. This process can detect temperatures of up to 1200°C.

Temperature measurement with thermocouples is among the most common techniques today. Installing a thermocouple into the tool or workpiece allows for a point-wise determination of the temperature field (Fig. 3.29). The thermocouples included are classified as encapsulated thermocouples, sheathed thermocouples and single filament thermocouples. Thermocouples can be applied in blind holes in the tool [Küst56, Qure66, Abra97] or in the workpiece [Osul02]. Temporal resolution is influenced by the response time of the thermocouple and heat transfer between the thermocouple and the device under test. These techniques generally have low temporal resolution. Also problematic is the contact heat transfer resistance between the surface under test and the thermocouple due to the roughness of the bore. This causes a difference in temperature between the measurement surface and the thermocouple. In the case of sheathed thermocouples with isolated measuring points, there is also the distance between the thermocouple surface and the internal measurement point. Due to the extremely high temperature gradients with short test times characteristic of cutting processes, this can lead to much lower measurements. The maximum values dominant in the friction zones cannot be measured in this way. Thermal compounds are used to improve heat transfer between the thermocouple and the surface. Another disadvantage is that direct contact between the thermocouple and the test object is necessary and that the holes used to position the thermocouples can significantly affect the distribution of temperature.

The most important techniques in radiation measurement, which determines temperature by measuring the heat radiation emitted from a surface, are pyrometry and thermography. Pyrometry is the contact-free determination of absolute temperature by measuring the inherent radiation of a body without spatial scanning of the object field. Thermography provides a pictorial representation of temperature distribution. Radiation techniques have decisive advantages compared with thermoelectric

methods: the time resolution is much higher (whereby pyrometers are principally faster than infrared cameras), and they are also contact-free.

One significant problem when measuring for an exact absolute temperature with a radiation method is the dependence of the radiation emitted on the grade of emission of the surface. Since the emission grade is the function of many factors like temperature, wavelength, angular position, material and surface condition, calibrating the measurement device for a particular surface is very difficult. The precision of total radiation and broadband partial radiation pyrometers are especially influenced by factors that alter the spectral grade of emission of the surface. In cutting, effects such as surface roughness and oxidation influence the grade of emission of different surfaces greatly. To limit the influence of the grade of emission on measured temperatures, narrow-band partial radiation, two-colour and multi-colour pyrometers have been developed. The two-colour pyrometer (Fig. 3.31) has the advantage that the spectral grades of emission ε_1 and ε_2 of the surface need not be known. Since the two selected wavelengths lie directly next to each other, $\varepsilon_{\lambda 1} \sim \varepsilon_{\lambda 2}$. An error in measurement will only result if both wavelengths λ_1 and λ_2 differ greatly. Further advantages of this principle are that the measured temperature is independent of signal dampening, due to dust for example, so long as both signals are dampened equally. Moreover, the temperature of objects that are smaller than the optical field of vision can be measured without error [Müll85].

Thermography with infrared cameras can be used as an alternative to pyrometrical measurements. The advantage to this is the pictoral representation of temperature information. Commercial cameras usually work with long wavelengths and large broad-bands, which makes it possible to measure lower temperatures but which also has a negative effect on the attainable accuracy. Scanning cameras that work with a single detector are too slow for fast processes. Some high-speed infrared cameras

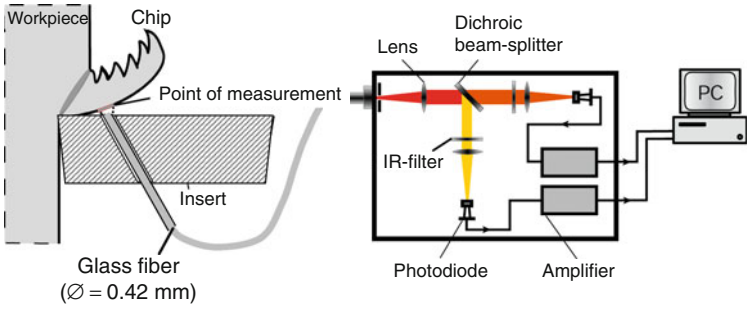

Characteristics

- Measurement of two discrete wavelength bands $\lambda_1 = 1.7$ µm, and $\lambda_2 = 2$ µm which are set into ratio
- High temporal resolution (approx. 2 µs)
- Independence from grade of emission (no calibration required)
- Large range of temperature measurement (250–1200 °C)
- Contact free measurement

Fig. 3.31 Build-up of a two-colour pyrometer in principle, acc. to MÜLLER [Müll85]

offer integration times in the range of microseconds, making it possible to capture fast processes without motion blur.

One major problem in the metrological determination of cutting temperatures, besides poor accessibility, is the limited local resolution of the available measurement techniques as well as the small range (only a few micrometers) within which the maximum temperatures arise. Local temperatures in the boundary layer between the cutting tool material and the sliding chip also cannot be captured with existing measurement methods. Promising attempts to determine thermal tool load more accurately than previously have been made with sensors in thin-film technology, which are applied to tool contact zones and determine temperature distribution within the contact zones during the machining process [Zieb95, Töns95, Kloc97]. This technology is however not yet suitable for cutting processes with high wear. Another highly promising method for determining temperatures in the boundary layers between the material and the cutting tool material is the implantation of a window made of diamond in the tool contact zone. Heat radiation emitted from the chip bottom side passes through the window via a mirror integrated into the chisel holder and reaches an infrared camera [Müll96].

A direct comparison of the temperatures measured by various authors is only rarely possible, since experimental conditions generally deviate from each other. There are numerous parameters that may have an effect on temperature: the type of cutting process, materials, cutting tool materials, possible coatings of the cutting tool materials, the use of cutting fluids and cutting parameters such as feed, cutting speed, depth of cut and cutting section geometry. Moreover, the measurement position is also crucial as well as metrological parameters like local or temporal resolution. The duration of the cutting process and the measurement time must also be taken into consideration.

Cutting speed clearly has the greatest influence on the maximum temperatures that arise in the contact zone between the chip and the tool. In the case of the basic process, most measurements indicate an apparent rise in temperature at low to average cutting speeds, while at high speeds there is an approximately constant temperature level.

3.6.1 Influence of the Geometry of the Cutting Section

Depending on the cutting task at hand, we can select from a diverse array of cutting section geometries. Geometry selection depends on

- the cutting tool material,
- material,
- cutting parameters and
- tool geometry.

Typical tool angles in steel cutting are given in Fig. 3.32. Determining the tool angle always involves a compromise that can only do approximate justice to various requirements.

Figure 3.33 shows how a change in cutting section geometry influences cutting parameters.

Geometry of cutting section / Cutting tool material	Tool orthogonal rake angle γ_o	Tool orthogonal clearance α_o	Cutting edge inclination λ_s	Cutting edge angle κ_r	Tool included angle ε_r	Corner radius r_ε
High speed steel (HSS)	–6° to +20°	6° to 8°	–6° to +6°	10° to 100°	60° to 120°	0.4 to 2 mm
Cemented carbide	–6° to +15°	6° to 12°				

Fig. 3.32 Tool angle for machining of steel

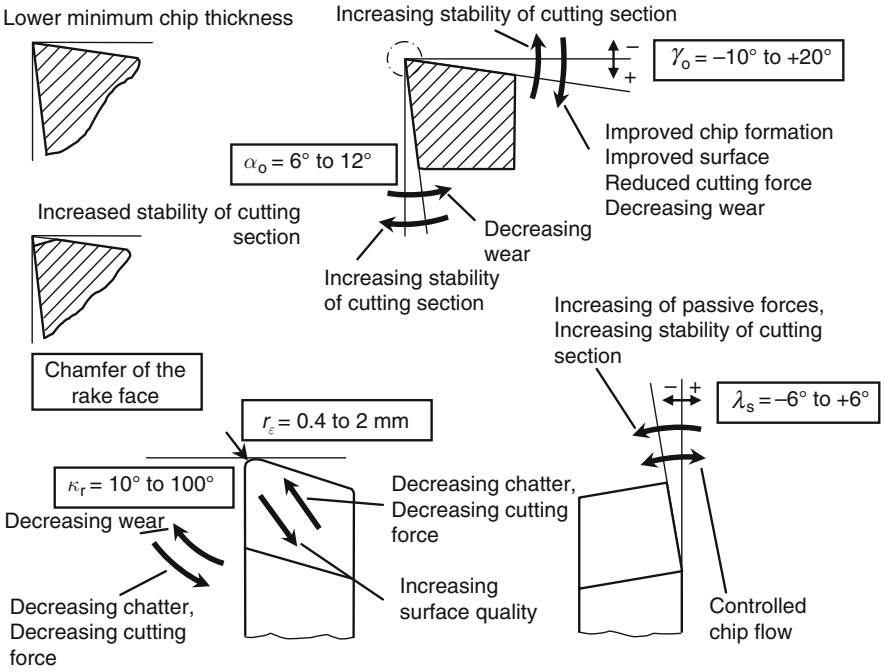

Fig. 3.33 Influence of cutting edge geometry on characteristic machining values

3.6.1.1 Tool Orthogonal Clearance α_o

Wear on the flank face (denoted by the width of flank wear land VB) is mostly determined by the size of the tool orthogonal clearance. If it is large, the cutting section is weakened in two respects: a heat build-up can ensue in the tool that can possibly lead to impaired or loss of hot hardness; also, if the wedge angle is too small, this increases the danger of breaking on the cutting edge. If $\alpha_o \rightarrow 0°$, surface

wear increases because pressure weldings appear on the contact areas of the friction partners to a greater extent.

3.6.1.2 Tool Orthogonal Rake Angle γ_o, Wedge Angle β_o

The tool orthogonal rake angle γ_o can, in contrast to α_o, be either positive or negative. It is responsible for the detachment of the material to be cut. The size of the tool orthogonal rake angle γ_o affects the stability of the wedge; highly positive tool orthogonal rake angles can thus lead to tool breakage as a result of cutting section weakening. The primary advantages of a positive tool orthogonal rake angle are the low cutting and feed forces as well as a usually improved workpiece surface quality. However, a chip flow that is supported by a positive tool orthogonal rake angle often has insufficient chip breakage (tendency towards the formation of continuous chips). Negative tool orthogonal rake angles increase cutting edge stability (used for example for planing and machining workpieces with apertures, rolling skin or cast skin). The thereby increased deformation of the passing chip and the large cutting forces result in a high temperature load on the cutting section. Increased crater wear appears on the rake face, which can lead to a decreased tool service life. Together with the wedge angle β_o, the tool orthogonal rake angle γ_o and the tool orthogonal clearance form a right angle α_o (Fig. 3.8).

3.6.1.3 Tool Included Angle ε_r

Due to the tool stability that is desired under extreme cutting conditions, the tool included angle ε_r should be as large as possible. Small tool included angles are required especially for copier and NC machining. The possible range is limited by specifying the position of the major cutting edge and by making sure that the angle between the minor cutting edge and the feed direction is at least 2° in order to avoid subsequent shaving of the minor cutting edge on the workpiece.

3.6.1.4 Cutting Edge Angle κ_r

At constant feed and depth of cut, the width of undeformed chip b increases with decreasing κ_r. This causes the specific cutting edge wear to sink, so small cutting edge angles are used especially to machine high strength materials in order to keep tool load and wear low. On the other hand, the passive force F_p rises with decreasing κ_r, increasing the danger of clattering vibrations due to growing instability of the cutting process.

3.6.1.5 Cutting Edge Inclination λ_s

A negative cutting edge inclination can stabilize the cutting process to a large extent since the lead of the tool does not take place on the cutting edge but rather towards the middle of the cutting edge. This results in an improved load profile, so that the danger of cutting edge breakage due to local overloading is reduced. First cuts that have minimal loads are of particular importance especially in the case of interrupted

cross sections (e.g. in milling or planing) as well as in the machining of cast iron and forged parts (workpieces with transverse drill holes, shrinkage cavities).

Negative cutting edge inclinations induce large passive forces, which must be absorbed by the machine tools (stiffness perpendicular to the main spindle!).

The cutting edge inclination also influences the direction of chip flow. A negative cutting edge inclination can result in the chip getting diverted to the workpiece surface, decreasing the surface quality.

3.6.1.6 Corner Radius r_ε

The corner radius to be selected depends on the feed f and the depth of cut a_p. Together with the selected feed, it influences the attainable workpiece surface quality to a great extent (see Sect. 7.2.3), whereby the following relation is approximately true:

$$R_\mathrm{t} = \frac{f^2}{8r_\varepsilon} \tag{3.13}$$

Large corner radii improve the surface quality and cutting stability. Small corner radii have the advantage of a smaller clattering tendency due to smaller passive forces.

3.7 Wear

During the cutting process, deformation, separation and friction processes take place in the area of the cutting edge. The cutting tool materials used are subject to an extremely complex load collective characterized by high compressive stresses, high cutting speeds and high temperatures.

Using cutting parameters common in practice, cutting tools reach the end of their service life because of continuously increasing wear on both rake and flank faces. This is explained as the progressive loss of material from the surface of a solid body, brought about by mechanical causes, i.e. contact and relative motion of a solid, liquid or gaseous counter body.

3.7.1 Wear Mechanisms

The main mechanisms that cause wear are adhesion, abrasion, tribochemical reactions and surface disruption (Fig. 3.34).

3.7.1.1 Abrasion

Abrasion occurs when rough areas of the counter body or particles present as intermediate material or also as counter bodies penetrate into the surface of the cutting tool material and simultaneously make a tangential motion, producing scores and

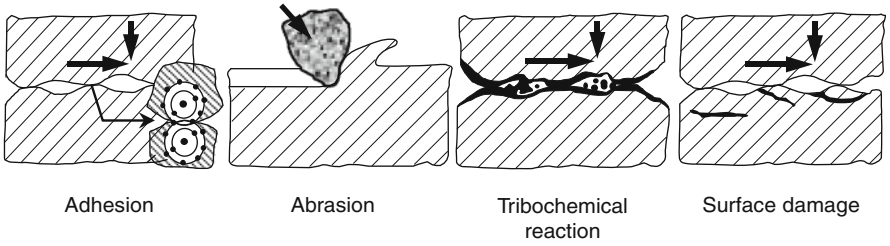

Fig. 3.34 Schematic illustration of the four main mechanisms of wear, acc. to ZUM GAHR [ZumG92]

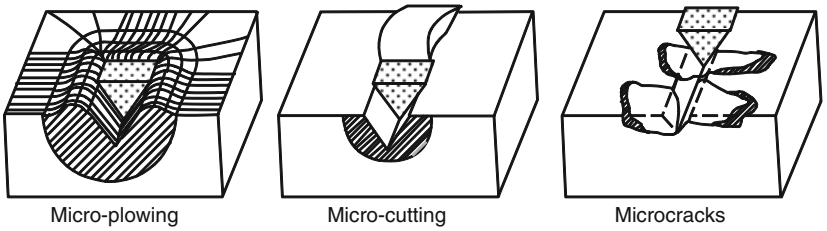

Fig. 3.35 Types of material damages caused by abrasive parts, acc. to ZUM GAHR [ZumG87]

micro-cutting. The various forms of abrasion are designated as groove, fluid erosion, mill, notch or blast wear. Often, the term "groove wear" is used synonymously with the term "abrasive wear" [Habi80, Czic06].

In the case of groove wear, hard areas of roughness or hard particles penetrate into the surface of the stressed material, creating scores or grooves by a sliding movement. Wear can be caused by a rough, compact counter body (counter body grooving) or by loose particles in the case of sliding load (particle grooving).

The process of material damage can be subdivided into micro-plowing, micro-cutting and microcracks (Fig. 3.35). Micro-plowing and micro-cutting are the predominant wear processes in the case of ductile materials. In the case of micro-plowing, the material is plastically deformed within the wear groove and pushed towards the groove edges. In the ideal case, no material is removed. This can however occur if the material is repeatedly pushed to the groove edges due to the simultaneous effect of many abrasive particles or due to multiple effect of a single particle, and the material finally fails due to fatigue. Ideal micro-cutting leads to material removal in the form of a chip, the volume of which is equal to the volume of the wear groove created. In the case of brittle materials, microcracks also arise. Material particles are hereby generated by means of cracking and crack growth in the stressed surface. The volume of the wear particle created in micro-cracking is much larger than that of the continuous wear groove [ZumG87, ZumG92, Habi80].

3.7.1.2 Adhesion

Adhesion is defined as the formation of bonds between certain molecules [Erin90, ZumG87]. As a wear mechanism this process is understood as one in which atomic bonds (e.g. in the form of micro-welds) are formed in the contact zone between the material and the cutting tool material. These bonds are then deformed, reinforced and sheared off during a tangential motion of the friction partners.

The process of adhesion (i.e. the formation of micro-welds between two friction partners) can come about by atomic interaction (chemical adhesion) between the partners, such as thermally induced diffusion processes, electron exchange or electric polarisation. It can also result from mechanical snagging (mechanical adhesion) of the workpiece material, which has plastically become extremely deformable under high temperatures, with the cutting tool material [Tell93].

By means of adhesion, particles can be transferred from one wear partner to the other. If this transfer is the primary cause of wear, it is sometimes referred to as adhesive wear, although other wear mechanisms are usually also involved in the formation of loose wear particles [Habi80].

Adhesion is a pairing property that depends on the characteristics of the base and counter bodies. Whether a material has the propensity to adhesion can only be answered with reference to the material of the counter body, with which it may either form strong, weak or no adhesion bonds at all [Habi80].

The strength of an adhesion bond is described by the adhesion coefficient. This is defined as the quotient of the normal force F_N with which two solid bodies in relative motion are pressed against each other and the opposing force F_A that must be applied to undo the bond formed by adhesion [Habi80, Andr59, Siko63].

The propensity of solid bodies to form adhesion bonds can be evaluated with the help of their surface energy. Contact angle measurement is one method for ascertaining the surface energy of solid bodies. [Bobz00] describes a measurement process that makes it possible to compare the surface energies of coating systems with respect to their polar and dispersive parts. Since it is the polar energy share that is primarily responsible for the propensity of a solid body to adhesion, the surface energy of cutting tools (i.e. especially that of the coating system) should have as little polar energy as possible in order to minimize that propensity [Bobz00, Kloc05].

During chip formation, new material surfaces are generated that, without adsorption or reaction boundary layers in statu nascendi, come in a chemically highly active state into contact with the tool surface under high pressures and temperatures, approaching that surface on the atomic level. Plastic deformation processes lead to the formation of large real contact areas. The cutting process thus provides very good opportunity for the appearance of adhesively caused interactions [Bömc89, Neis94, Erin90].

3.7.1.3 Tribooxidation

The term “tribooxidation” refers to chemical reactions of the cutting material and the material with components of the intermediate material or the surrounding medium as a result of activation caused by friction. Tribooxidation changes the properties

of the external boundary layer. Reaction products can be formed that are either removed with the chip or remain stuck to the cutting tool material as a coating. Wear can be increased or reduced by this. Whether tribooxidation increases the amount of wear essentially depends on the hardness of the reaction products formed in comparison with the hardness of the cutting material. A decrease is especially possible when the reaction layers prevent direct metallic contact between the base and counter bodies, limiting the effect of adhesion [Erin90, Habi80, Tell93].

3.7.1.4 Diffusion

Diffusion is the thermally activated change of position of individual atoms [Horn67]. This involves a temperature-dependent physicochemical process in which the wear resistance of the cutting tool material can be reduced by foreign substances diffusing with it or its own components diffusing away from it. The diffusion of atoms from the tribologically loaded areas of the tribopartners leads on the one hand to a direct loss of material, which is usually very small but can still certainly be measured as a quantity of wear; however, much more serious is the potential reduction of the wear resistance of cutting tools by the diffusion of certain alloying elements. Diffusion of essential alloying elements can lead to decreased hardness and thus to reduced resistance of the cutting tool material to abrasion [Neis94, Erin90, Habi80].

The high pressures and temperatures in the contact zones characteristic of the cutting process provide an ideal setting for diffusion processes between the material and cutting tool material. Diffusion processes appear especially when high cutting speeds are used, thereby leading to high temperatures in the contact zone. In the area of the contact zone, the cutting tool material and the material approach each other on the atomic level. Furthermore, there is a difference in concentration due to the differing compositions of the material and the cutting tool material which also is preserved in the material because of the constantly added chip [Neis94, Erin90].

3.7.1.5 Surface Damage

Surface damage occurs as a result of tribological alternating stresses. In the stresses surface areas, alternating mechanical stresses lead to structural changes, fatigue, cracking, crack growth and even to separation of wear particles [Habi80].

As opposed to abrasion, in which wear particles can be formed by a single stress process, surface damage is usually preceded by a longer incubation period during which no measurable wear occurs. In this period, the formation of wear particles by means of structural changes as well as cranking and crack growth is prepared [Habi80].

3.7.2 Causes of Wear

Friction processes in tool contact zones are comparable to those of dry friction in a vacuum. Together with extraordinarily high mechanical and thermal stresses, the tool is generally worn out quickly [Rabi65, Krag71, Opit70a, Opit70b].

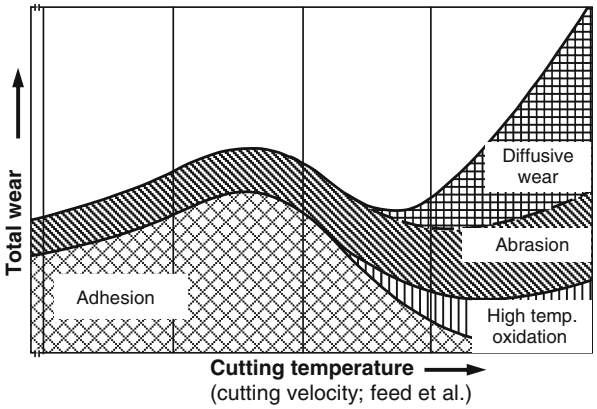

Fig. 3.36 Causes of wear in cutting processes

According to current information, the following separate causes can be given for the collective term "wear" (Fig. 3.36):

- mechanical wear (abrasion),
- the shearing off of adhered material
- damage to the cutting edge due to mechanical and thermal overstress,
- diffusion,
- scaling.

These processes overlap to a large extent and are only partially separable from each other with respect both to their cause and to their effect on wear [Opit67, Köni65, Ehme70b, Ehme70c].

3.7.2.1 Mechanical Wear (Abrasion)

Mechanical wear or abrasive wear occurs at both low and high cutting speeds. Groove wear in the form of counter body or particle grooving can be seen as the dominant form of wear in this category. In the case of counter body grooving, tribological stress on the cutting tool material is based on the abrasive effect of hard particles fixed on the contact surface of the workpiece or the chip. These particles can originate from the workpiece material (oxides, carbides, nitrides) or be transferred by adhesion from the cutting tool material to the workpiece or chip bottom side. In the case of particle grooving, loose particles are the cause of wear. These can arise directly from abrasion (micro-cutting, microcracks) or from surface disruption. However, these may also be adhesion particles or products of tribooxidation removed by abrasion or surface fatigue. Due to the high pressures and temperatures that predominate in the contact zones on both rake and flank faces, we must presume that the loose particles generated are pressed into the softer counter bodies flowing by them, contributing to further wear by counter body grooving.

Due to abrasion or surface disruption on the cutting edge or in the contact zones on the rake and flank faces, cutting tool material particles that have broken away from the cutting tool material flow over the rake or flank face under high pressure. This can cause further wear by micro-cutting or microcracks. This process, also called "self-wear" [Ehme70a], is of particular importance especially with respect to the formation and development of flank face wear.

3.7.2.2 Shearing-Off of Adhered Material Particles (Adhesion)

In the case of micro-welds being sheared off, material separation can occur in the boundary layer, within one or within both bodies. The term adhesive wear is used as soon as material is separated in the cutting tool material. Adhesion is also responsible for the formation and growth of built-up edges, in which material is transferred from the material to be cut to the cutting tool [Erin90, Habi80, ZumG87].

Ferritic and austenitic steel materials have a high propensity to adhesion with the cutting tool material. The reason for this is above all the high plastic deformability of these materials. The high ductility of ferritic materials is based above all on their relatively low strength, in the case of austenitic steel materials on their face-centred cubic crystal lattice.

Tungsten carbide, the basis of hardness and wear resistance in conventional WC-Co cemented carbides, has a hexagonal crystal structure. On the other hand, the crystal lattice of the binding metal cobalt is face-centred cubic above 690 K, which is favourable for adhesive processes. The titanium-based coating systems commonly deposited on cemented carbides also have face-centred cubic structures, resulting in a strong tendency to adhesion when machining austenitic steels. The types of wear resulting from this strong adhesive tendency can range from material bonding on the rake and flank faces to de-coating of coated tools in the area of the contact zone.

Built-up edges are highly reinforced layers of the machined material that take over the function of the tool cutting edge as bondings on the tool. This is made possible by the property of certain materials to harden during plastic deformation. The material adhering to the cutting edge is deformed by chip pressure, making it very hard. This makes it possible for it to take over the function of a chip-removing tool.

Depending on the cutting conditions, built-up edge particles slip periodically between the flank face and the cutting surface. In the case of high hardness and removal frequencies up to about 1.5 kHz, these particles lead to increased flank face wear and considerably deteriorate the surface quality of the workpiece (Fig. 3.37). Since the chip is diverted with the built-up edge and not the rake face, crater wear is usually negligible.

Figure 3.38 shows a wear-cutting speed function (VB-v_c graph). According to it, flank face wear does not increase with cutting speed continuously, but has at least two distinct extremes [Opit64]. Wear first reaches a maximum at the cutting speed at which the built-up edges reach their largest dimensions. A wear minimum appears at the cutting speed at which no more built-up edges form.

Flank face wear decreases after exceeding the maximum, despite higher cutting speeds. This can be ascribed to the fact that reinforcement of the built-up edge

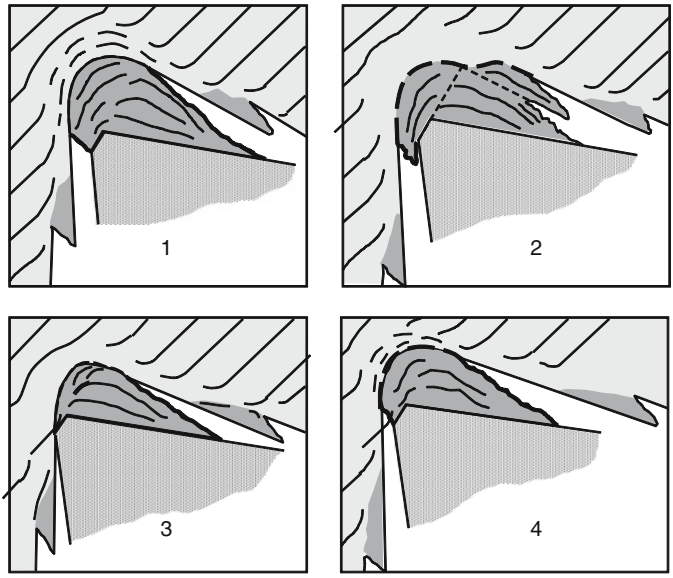

Fig. 3.37 Scheme of the periodic growth of build-up edge

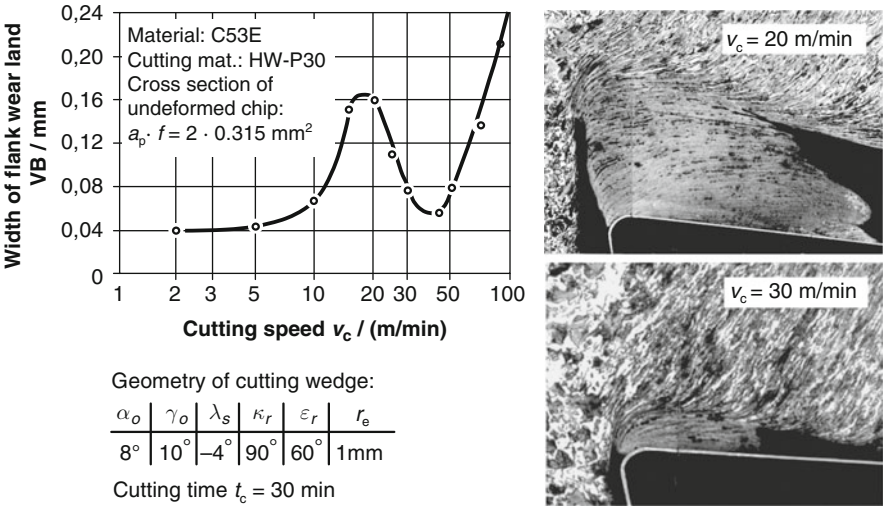

Fig. 3.38 Wear on flank face and growth of build-up edge

begins to decrease as a result of recrystallization processes. It becomes unstable and no longer migrates partially between the cut surface and the flank face, but as a whole across the rake face.

The position of the maxima and minima of the VB-v_c graph is contingent on temperature. It is shifted to lower cutting speeds by any kind of measures taken

to increase the cutting temperature (e.g. higher feed, smaller tool orthogonal rake angle, higher material strength). Measures to reduce the cutting temperature (e.g. cooling) shift the extremes accordingly to higher cutting speeds [Opit69, Peke74].

3.7.2.3 Mechanical and Thermal Overstress

Damage to the cutting edge, such as breaking, parallel cracks, comb cracks or plastic deformation, is the consequence of mechanical or thermal overstress.

Cutting Edge Chipping

Large cutting forces lead easily to breaking on the cutting edge (cutting edge chipping) or corner if the wedge angle or tool included angles of the tool are too small or the cutting tool material used is too brittle. In the case of such breaking, the profile of the fracture surface is determined by the direction of the cutting force [Köni75]. Cut interruptions can also lead to breaking, especially when tough materials are being cut, the chips of which tend to stick.

Small amounts of breaking occur when the workpieces contain hard non-metallic inclusions that originate during deoxidation of the steel [Opit64a, Opit66, Opit62]. Sintered oxides and more wear-resistant types of cemented carbide are sensitive to this type of local overstress, especially in the case of manufacturing processes with relatively small cross-sections of undeformed chip (e.g. reaming or shaving).

Distinct breaking of cutting tool material on the major and/or minor cutting edge can also be caused by chips striking against the cutting edge or during the rotation of shaft sections because of chip jamming between the cutting insert and the workpiece. Breakage of the cutting edge can occur both on the top and bottom sides of the insert.

Parallel Cracks

In the case of interrupted cuts (e.g. milling), the cutting tool material is subject to strong mechanical alternating stress. This dynamic pressure threshold load can lead to fatigue failure. Quick consecutive cutting force changes lead, especially in the case of milling with cemented carbide tools, to parallel cracks (Fig. 3.39).

The quickly alternating stress in the formation of lamellar chips can also lead to parallel crack formation if a critical stress cycle is exceeded [Domk74, Beck69], e.g. when cutting titanium materials.

Comb Cracks

Comb cracks are a form of damage to the cutting edge as a result of thermal alternating stresses (Fig. 3.39). Such stresses originate mainly while working with interrupted cuts.

During tool engagement, the cutting edge quickly heats up to high temperatures. It cools down after the tool exits the workpiece. The difference between the highest and the lowest temperature depends, among other things, on the material, cutting

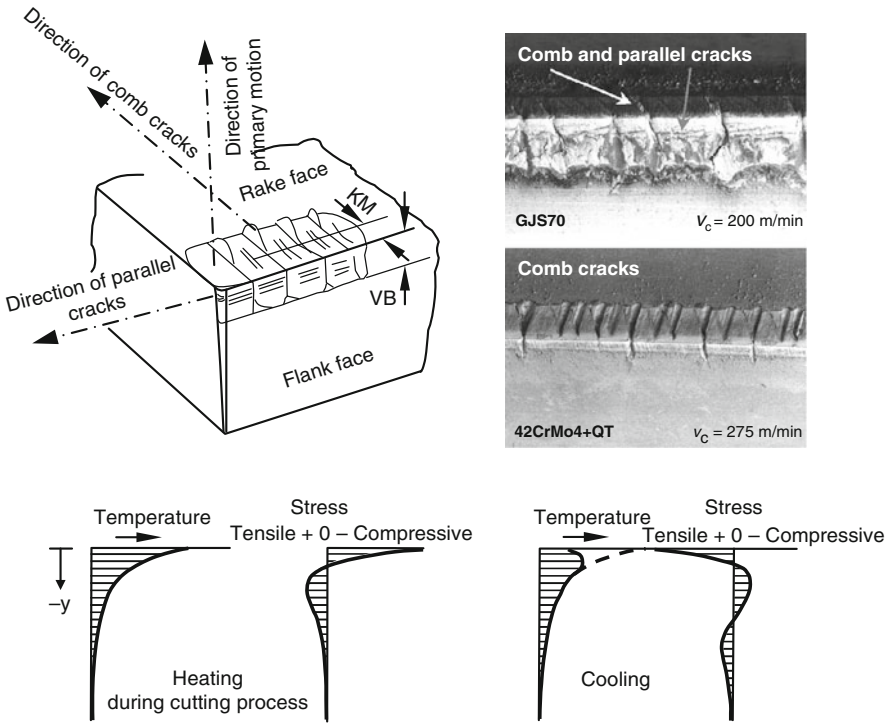

Fig. 3.39 Comb and parallel crack formation in milling, acc. to VIEREGGE [Vier59]

conditions and the ratio of the paths covered in the material and in the air. In the case of interrupted cuts, the use of cutting fluids is particularly important with respect to the size of the temperature difference because it has a much larger quenching effect than air. Cooling is advantageous to the formation of comb cracks in the case of cemented carbides and ceramic cutting tool materials. The profile of the comb cracks is aligned with that of the isotherms of the temperature field in the cutting part.

The comb cracks arising in the cutting part during milling or also in short-cycle turning are generally temperature change cracks. These should be distinguished from thermoshock cracks such as develop during turning or milling while using cutting fluid. Thermoshock cracks are formed by a nonrecurring steep temperature change, while temperature change cracks form only gradually in the cutting part in the course of the cutting edge engagement. While in the case of thermoshock the thermally caused tensile strain arising in the contact zone exceeds the strength of the cutting tool material and leads directly to cracking, the stresses leading to the formation of temperature change cracks are below the strength of the cutting tool material. The development of temperature change cracks thus requires several periodic temperature changes as a rule.

Due to the high energy level thermoshock cracks propagate with greater speed. Crack growth is largely transcrystalline. Depending on the stress level, they can acquire very large depths in the cutting tool material (> 1 mm), thus leading to considerable weakening of the cutting edge [Gers98].

Temperature change cracks can be observed in both wet and dry cuts. Besides the amount of thermal load, the cutting cycle and the number of cutting cycles play a decisive role in their formation. The use of cutting fluids leads to a strong reduction of the amount of cutting cycles required for cracking [Gers98].

Depending on the bending stress which the cutting edge is subject to during the cutting process and which are superimposed over thermally induced stresses, the cracks become larger with increasing numbers of cutting cycles. With a corresponding output length, they can relatively quickly achieve a critical size leading to fracture. As a result of the notching effect coming from the crack, they can also become the source of further cracks [Gers98].

Plastic Deformation

Plastic deformation of the cutting edge arises when the thermomechanical stress effecting the tool cutting edge exceeds the deformation resistance of the cutting tool material. The influencing parameters are the strength of the material to be cut, the cutting parameters, the geometry of the insert and, on the part of the cutting tool material, its high temperature properties like hardness, compressive strength and creep behaviour.

Cutting edges made of tool steel or high speed steel deform the stronger the smaller the difference is between the temperature of the cutting edge and the annealing temperature of the cutting tool material. Plastic deformations also appear in the case of cemented carbides and cermet, however only at higher temperatures (cutting speeds) and under higher forces as is the case for tool or high speed steels. Cemented carbides deform more the more binder phase there is, usually cobalt.

Plastic deformation of the cutting edge results in a considerable increase in wear and can lead to sudden disruption of the tool by cracking and shearing off of the cutting edge. It thus limits above all the cross-section of undeformed chip and cutting speeds applicable in rough turning.

3.7.2.4 Diffusion

In the case of heat wear resistant cemented carbide tools, diffusion wear must be expected at high cutting speeds and mutual solubility of the partners. Tool steel and high speed steel already become soft at temperatures at which diffusion can hardly manifest itself (e.g. about 600°C for high speed steel).

When cutting with uncoated cemented carbide substrates, the following reactions can occur (Fig. 3.40):

- diffusion of Fe into the binder phase Co,
- diffusion of Co into the steel, whereby Fe and Co form a gapless series of mixed crystals,

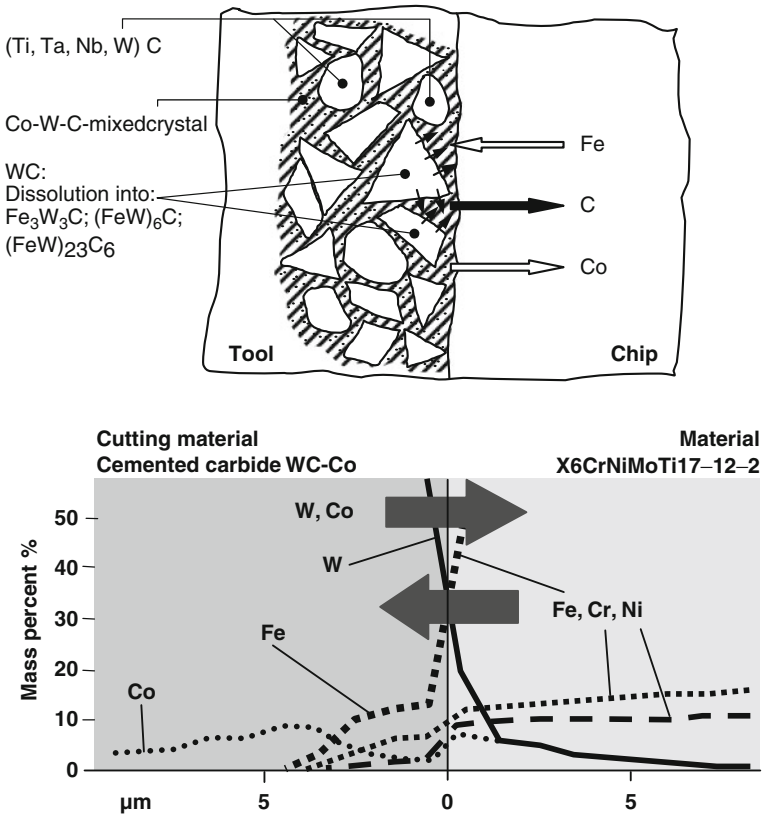

Fig. 3.40 Presentation of the diffusion phenomena in cemented carbide tools

- dissolution of tungsten carbide to form mixed and double carbides in the form of Fe_3W_3C, $(FeW)_6C$ and $(FeW)_{23}C_6$.

The carbon released during the dissolution of tungsten carbide migrates in the direction of lesser concentration, i.e. into the steel. The diffusion of carbon passes into the cobalt phase. The maximum solubility of carbon in cobalt is about 0.7% at 1200°C. In the presence of Fe the solubility is increased to 1.5–2%. The diffusing iron thus introduces two reactions, both of which accelerate dissolution. It lends itself to the formation of iron mixed carbides and increases the reception of carbon in cobalt, which is in turn the prerequisite for the dissolution of tungsten carbide.

The diffusion processes that are possible between cemented carbide and steel materials can be shown very effectively with the help of annealing tests. To this purpose, cemented carbide-material pairs were annealed at a temperature of 1100°C, a pressure of 12.6 MPa and a holding time of 2 h in a protective gas atmosphere of argon. Then the samples that were fused together on the contact surface were separated on an abrasive cut-off machine perpendicularly to the contact level, and

after these sample halves were grinded and buffed, the distribution of elements was analysed with a microprobe perpendicularly to the contact surface cutting tool material/material.

As the quantitative line scans in Fig. 3.40 show, diffusion phenomena take place under the selected annealing parameters between the uncoated cemented carbide and the austenitic steel material here selected. On the side of the steel material, there is a diffusion of iron, chrome and nickel into the cutting tool material. In the opposite direction (i.e. from the cutting material into the material) tungsten and cobalt diffuse.

The dissolution of tungsten carbide, the bearer of hardness and wear resistance, caused by the diffusion of iron into the cemented carbide leads to a weakening of the structure and lowers the resistance of the cemented carbide substrate against abrasion. The consequence of this is the formation of distinct crater wear (Fig. 3.41). Since diffusion phenomena depend on temperature, the cutting speed influences on an elementary level the speed with which crater wear develops. Uncoated cemented carbides can thus only be used at relatively low cutting speeds ($v_c < 100\,\mathrm{m/min}$). The cemented carbide substrate also has a serious effect on crater formation. Mixed carbides on the basis of titanium and tantalum/niobium have, in comparison to WC, a much higher chemical stability towards iron. Mixed carbides reduce the diffusion of iron into the cobalt binder phase, thus increasing the resistance of the cutting tool material to crater wear and increasing its heat wear resistance quite substantially.

The most effective way to reduce crater wear is coating the cemented carbide substrate. Cemented carbide layers seal the substrate surface. This prevents direct contact between the substrate and the material, thus reducing or suppressing diffusion phenomena. As the line scans of annealing tests in Fig. 3.42 show, diffusion processes between the cemented carbide substrate and the material can by all means still occur in the case of TiN or TiCN layers. In contrast, no more diffusion takes place in the case of the coated cemented carbide with Al_2O_3 as an intermediate layer. The aluminium oxide layer thus functions as a diffusion barrier. The elements iron, nickel and chrome are found in the ZrN surface layer, while tungsten and cobalt are in the TiN boundary layer (Fig. 3.42). In the aluminium oxide intermediate layer

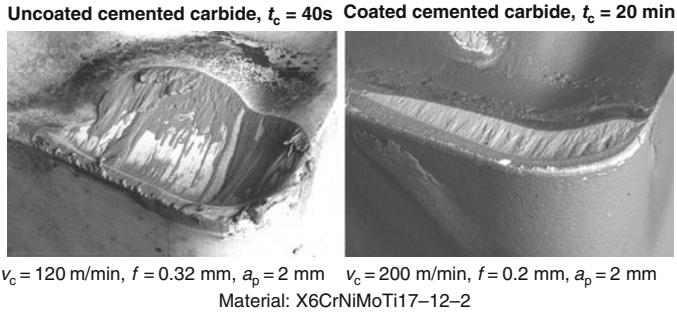

Fig. 3.41 Formation of crater wear on an uncoated and a coated cemented carbide, acc. to GERSCHWILER [Gers04]

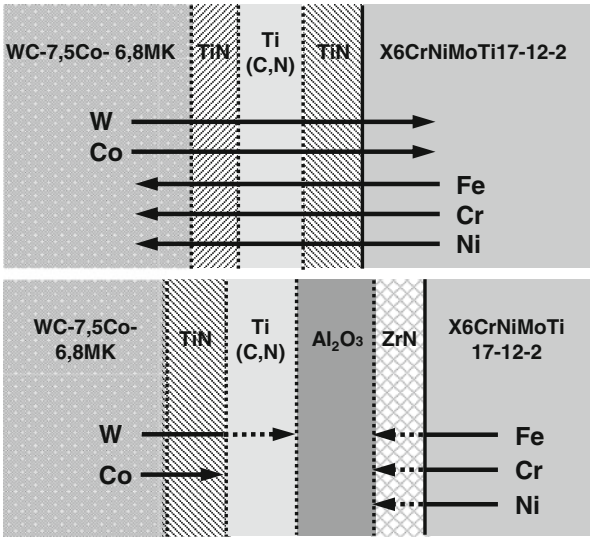

Fig. 3.42 Verification of the diffusion phenomena between coated cemented carbide and steel dependant on the coating system on the basis of annealing tests

the traceable amount of these elements is reduced to 0 mass-%. There is above all no indication that iron, chrome, tungsten or cobalt have diffused through the Al_2O_3 intermediate layer on the opposite side of that layer.

The observation that, excluding air or water, electrically isolated oxide layers function as diffusion barriers on cemented carbides as opposed to semiconducting nitride or carbon nitride layers can be explained as follows. In electrically isolating oxides like Al_2O_3 or HfO_2, only ion diffusion is possible, no migration of electrons or holes. The result of this is that "component diffusion" becomes impossible. "Component" refers to an atom or iron, which theoretically can be split into an ion and an electron. For reasons of electron neutrality, the iron atom cannot "release" its electrons outside the layer and then migrate through the layer as an ion. The consequence is that these oxide layers act as barriers as long as there is no way for electrons to get around it, and the transport of oxygen ions is also slow enough (in oxides this transport is empirically slower than cation transport by several orders of magnitude.) In semiconductive or conductive layers however, electrons can migrate through the layer together with the ions, leading finally to the iron element migrating through the layer to alloy with the substrate. Conversely, conveyance of Co or W into the chip is also possible. Diffusive transport is already possible at the temperatures prevalent on the tool during machining of > 800°C. The diffusion coefficients are indeed still small, but the necessary diffusion paths are very short.

While diffusion of iron through the cemented carbide layer into the cemented carbide substrate is indeed possible in the case of cemented carbides coated with TiN and TiCN, this diffusion is not as significant as is the case for uncoated substrates. As opposed to uncoated cemented carbides, the coat provides the substrate

with additional protection from the abrasive action of the flowing chip. Especially because they are much harder than the substrate, cemented carbide layers help to reduce abrasive wear to a significant extent. Cemented carbide layers thereby ensure the high performance level of coated tools and allow for much higher cutting speeds when cutting steel materials in comparison with uncoated cemented carbides (Fig. 3.41). But as soon as the hard material layer in the contact zone of the rake face has been rubbed off and the substrate exposed, diffusion processes now once again taking place between the substrate and the chip contribute, together with the abrasive effect of the chip on the substrate, to an acceleration of crater wear.

3.7.2.5 Scaling

If we examine a tool after cutting, we can recognize several annealing colours near the contact zones, indicating scaling (oxidation) of the cutting tool material. Scaling varies in importance depending on the cutting tool material alloy and cutting temperature (Fig. 3.43). Cemented carbides already begin scaling at 700–800°C, whereby

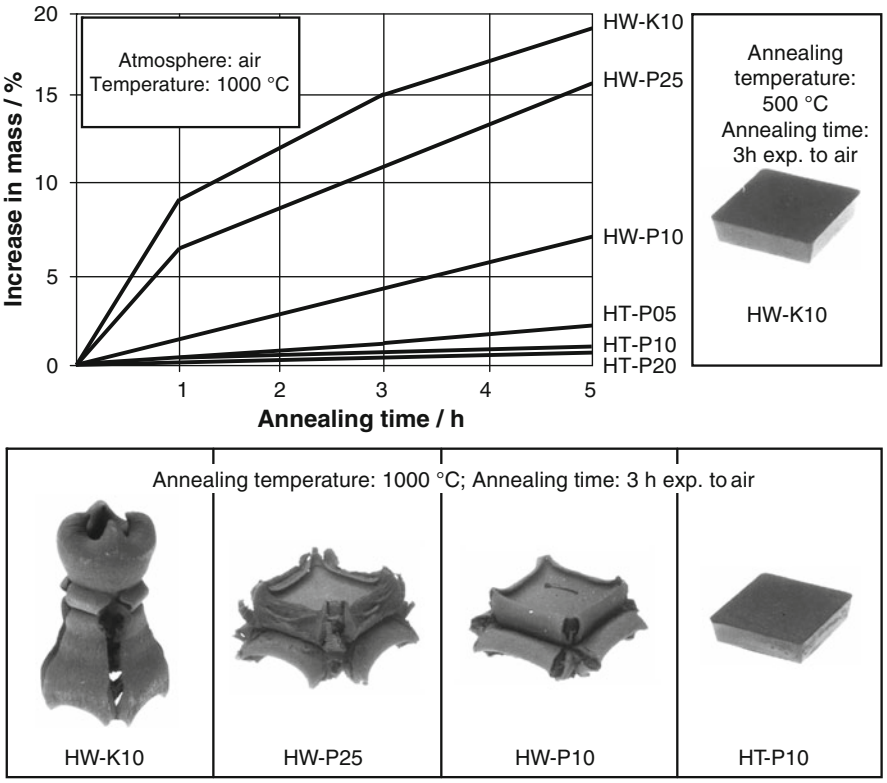

Fig. 3.43 Gain of weight during the annealing process in air dependant on the used cutting tool material

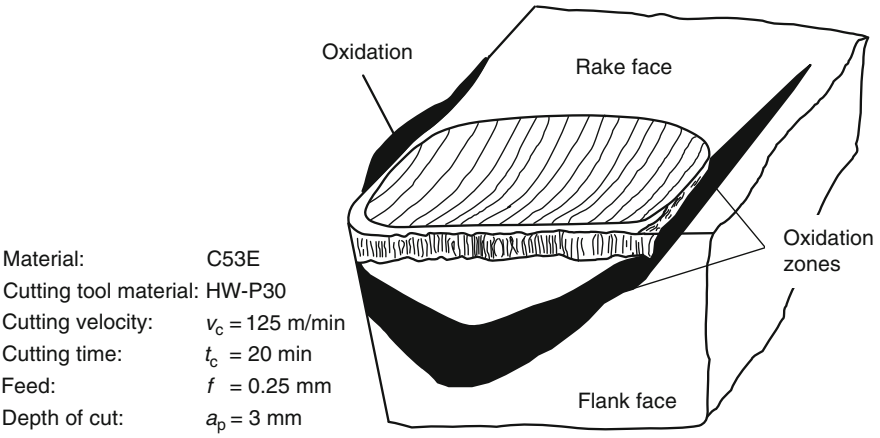

Fig. 3.44 Oxidation zones at a cemented carbide turning tool

those made of pure tungsten carbide and cobalt oxidize more than those alloyed with titanium carbide or other carbides [Kief65].

Even under the usual cutting conditions, an oxide film is formed on WC tools in the area of the cutting edge under the effect of the cutting temperatures and atmospheric oxygen. This film covers the areas to which atmospheric oxygen has free access, i.e. the ends of the contact zones on the flank face, minor flank face and rake face (Fig. 3.44).

The destructive effect of oxidation on the structure of cemented carbide can be observed especially clearly on the minor flank face. A complex tungsten-cobalt-iron oxide is formed that, as a result of its larger molar volume compared with cemented carbide, develops in a wart-like fashion and can lead to corner breaking [Köni75].

Scaling is of no practical importance for tool steels and high speed steels since their heat resistance is exceeded before their surfaces are oxidized more strongly.

3.7.3 Forms and Dimensions of Wear

Wear phenomena that are generated on the cutting part during cutting vary greatly depending on the type and duration of stress. Figure 3.45 shows wear forms that occur primarily on turning tools. The cutting part is worn on the rake face (crater wear) as well as on the major and minor flank faces (flank face wear) (Fig. 3.46). Depending on the cutting parameters and the combination of workpiece and cutting tool material, flank face wear tends to be strongest on the edge of the contact zone on the major and minor cutting edge of the tool, which continues on the rake face. Such “notch wear” is caused by the abrupt transitions of mechanical and thermal stress prevalent on the end of the contact area, the abrasive character of the sharp

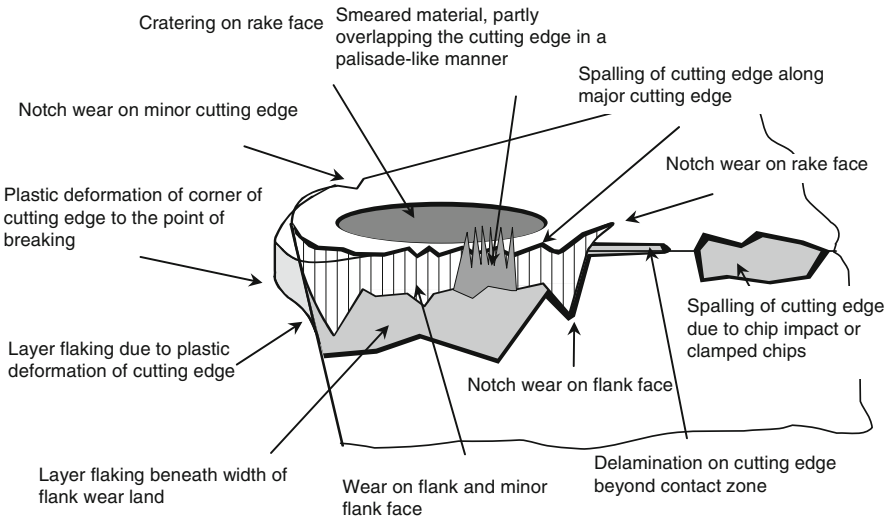

Fig. 3.45 Characteristic wear forms at the cutting part during the turning process

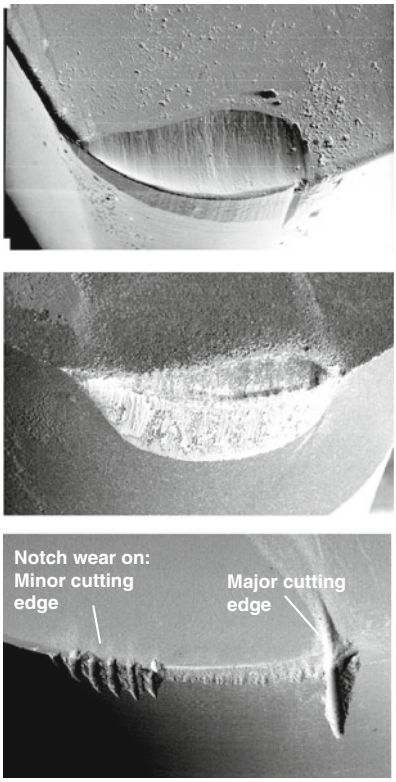

Cutting tool material: Cermet
Material: 42CrMo4+QT
Cutting parameters:
v_c = 400 m/min
f = 0.1 mm
t_c = 12 min
a_p = 0.5 mm
Insert geometry:
SPGN120308

Cutting tool material: PCBN
Material: Nickel-based alloy
Cutting parameters:
v_c = 300 m/min
f = 0.16 mm
t_c = 1.6 min
a_p = 0.3 mm
Insert geometry:
VBMW160412

Cutting tool material: Ceramic
Material: Nickel-based alloy
Cutting parameters:
v_c = 220 m/min
f = 0.16 mm
t_c = 2.3 min
a_p = 0.3 mm
Insert geometry:
RCGX090700T00515

Fig. 3.46 Examples for the formation of crater wear, flank face wear and notch wear dependent on the used cutting tool material and the machined material

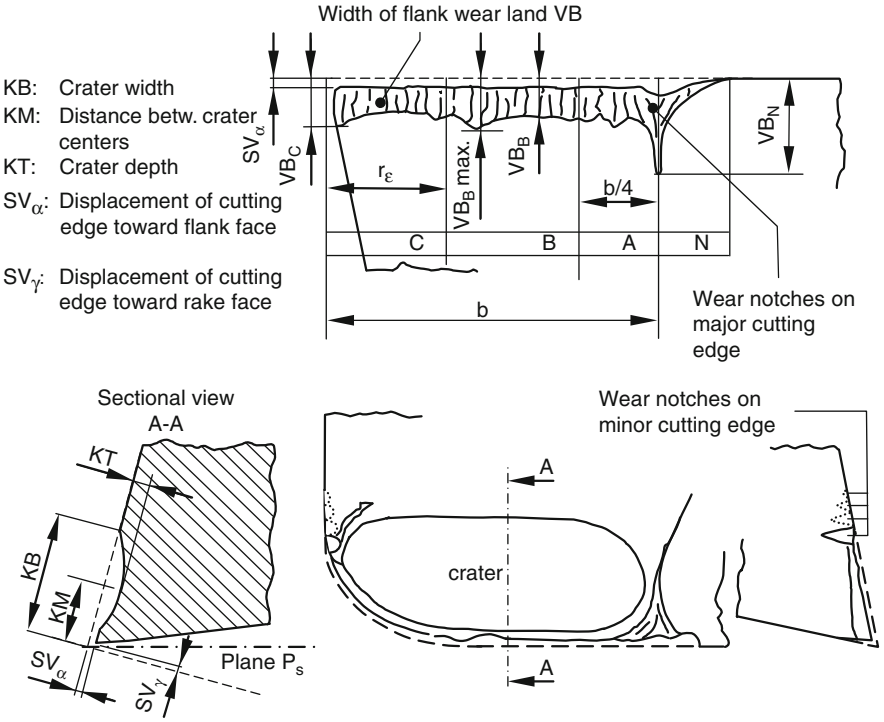

Fig. 3.47 Wear forms and measured quantities at the cutting part, acc. to DIN ISO 3685

chip edge or the feed comb and the tool edge as well as direct contact with the atmosphere (Fig. 3.46).

Figure 3.47 is a schematic representation of the dimensions of wear. In particular, we distinguish the width of flank wear land VB, the displacement of cutting edge toward flank face SV_α and rake face SV_γ, crater depth KT and the crater centre distance KM from which the crater ratio $K = KT/KM$ is formed.

3.8 Cutting Theory

3.8.1 Shear Plane Theory

The model representation of the shear plane is based on ideal cutting conditions. Required are:

- ideally sharp cutting edges,
- cutting edges that are not subject to wear,
- the representation of mechanical loads as substitute forces and
- ideal plastic material behaviour.

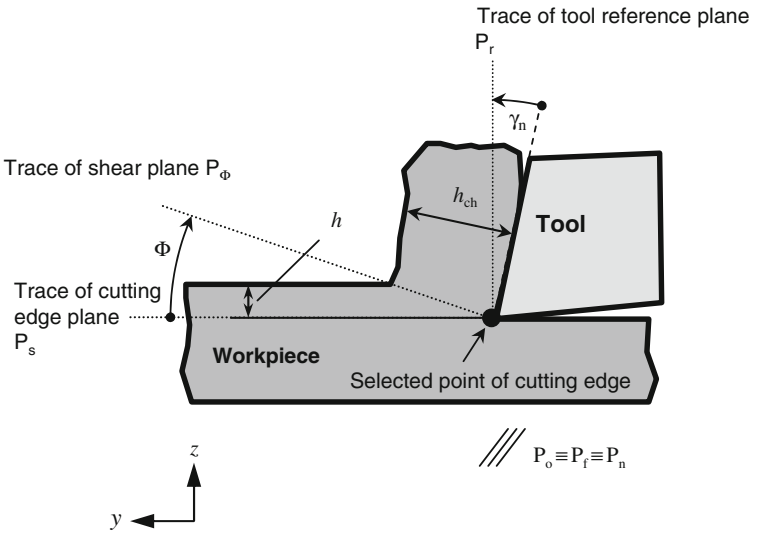

Fig. 3.48 Model representation of the shear plane

The chip formation theory derived from this model (shear plane theory) assumes that deformation takes place on only one plane, the shear plane. By definition, the shear plane passes through the selected point of cutting edge just like the tool-in-hand and tool-in-use reference system (Fig. 3.48).

In the following the shear plane P_Φ will be considered in the tool-in-hand reference system. This is a plane which is inclined toward the cutting edge plane P_s by the shear angle Φ.

The requirements made on process kinematics are fulfilled when:

- tool cutting edge angle $\kappa_r = 90°$
- tool inclination $\lambda_s = 0°$

We are thus assuming a free, orthogonal cut. The shear plane model has the advantage of making complicated cutting processes highly comprehensible.

If the effects of the corner radius and minor cutting edge are negligible in comparison with that of the major cutting edge, the theory of the shear plane can also be used for the bound cut.

With the shear angle we can macroscopically consider material and cutting tool material properties as well as thermal loads and friction conditions which predominate during contact of the chip with the rake face. Moreover, the shear angle establishes the relation between undeformed chip thickness h and chip thickness h_{ch}.

$$h_{ch} = \frac{\cos(\Phi - \gamma_n)}{\sin\Phi} \cdot h \tag{3.14}$$

By means of the shear angle we can now calculate the surface area of the shear area A_Φ in the shear plane:

$$A_\Phi = b \cdot \frac{h}{\sin\Phi} \tag{3.15}$$

The ratio of undeformed to deformed magnitudes is designated in forming technology as deformation. If the material is compressed and only the change in height is described, the term degree of compression is also used. This concerns volume consistency. In cutting theory, the term chip compression λ_h is used analogously [Krys39].

$$\lambda_h = \frac{h_{ch}}{h} = \frac{\cos(\Phi - \gamma_n)}{\sin\Phi} \tag{3.16}$$

The shear angle Φ is a purely theoretical quantity and should not be confused with the actual slip direction of the material, even if the shear surface and slip surface are nearly identical under certain marginal conditions.

In conclusion, to show that the theory of the shear plane makes it possible to calculate various quantities with complicated relations, three classical applications of shear plane theory will be described.

3.8.1.1 Calculation of Chip Speed

From simple trigonometric relations (law of sine) in the velocity plan, MERCHANT calculated the chip speed v_{ch} with the help of the shear angle Φ (Fig. 3.49) [Merc45].

$$|\vec{v}_{ch}| = \frac{\sin\Phi}{\cos(\gamma_n - \Phi)} \cdot |\vec{v}_c| \tag{3.17}$$

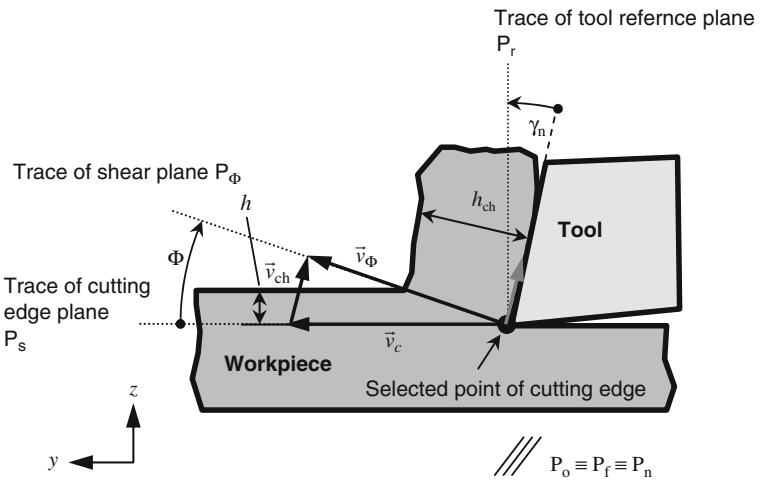

Fig. 3.49 Velocity plan, acc. to MERCHANT [Merc45]

The continuity equation can also be used to calculate chip speed v_{ch}. The idea behind this is that a mass flow flows through a control surface, in this case the shear surface. Assuming that the density of the material is not altered by mechanical and thermal load, we obtain:

$$\dot{m} = \text{const.} \Rightarrow |\vec{v}_c| \cdot A = |\vec{v}_{ch}| \cdot A_{ch} \tag{3.18}$$

From which follows:

$$|\vec{v}_{ch}| = \frac{h}{h_{ch}} \cdot |\vec{v}_c| = \frac{1}{\lambda_h} \cdot |\vec{v}_c| \tag{3.19}$$

3.8.1.2 Calculation of Resultant Force

It is assumed that the shear angle is a function of the shear stress in the shear plane, which will be shown in the following steps. In the first place we have:

$$\tau_\Phi = \frac{|\vec{F}_\Phi|}{A_\Phi} \tag{3.20}$$

The component of the resultant force in the shear plane, the shear force F_Φ, can be represented by the resulting resultant force F_z. With the help of the angle relations in the circle of THALES we obtain according to Fig. 3.50:

$$|\vec{F}_\Phi| = |\vec{F}_z| \cdot \cos(\Phi + \rho - \gamma_n) \tag{3.21}$$

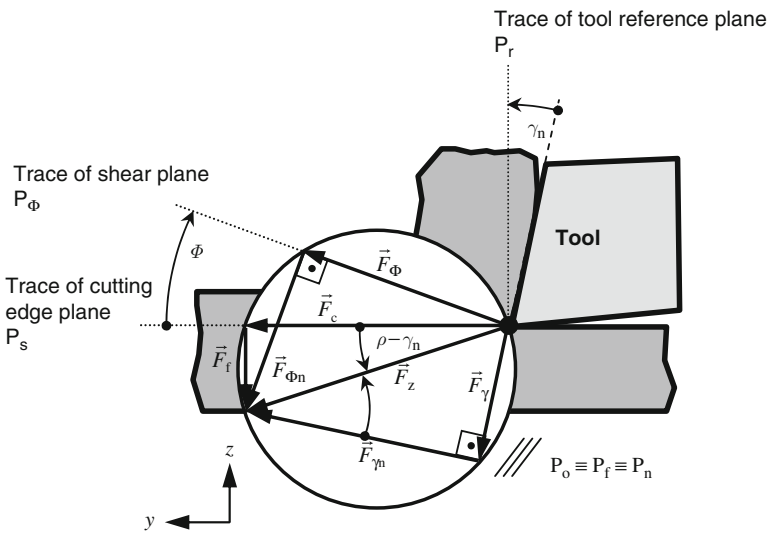

Fig. 3.50 Circle of THALES for the force diagram, acc. to MERCHANT

The amount of resultant force can now be calculated from Eqs. (3.20) and (3.21):

$$|\vec{F}_z| = \frac{\tau_\Phi}{\sin\Phi \cdot \cos(\Phi + \rho - \gamma_n)} \cdot b \cdot h \tag{3.22}$$

The functional relations of the values of the resultant force components cutting force and feed force can be taken from the circle of Thales (Fig. 3.50).

$$|\vec{F}_c| = |\vec{F}_z| \cdot \cos(\rho - \gamma_n) \tag{3.23}$$

$$|\vec{F}_f| = |\vec{F}_z| \cdot \sin(\rho - \gamma_n) \tag{3.24}$$

If we now insert Eq. (3.22) into Eqs. (3.23) and (3.24), the following is valid for the values of the resultant force components:

$$|\vec{F}_c| = \frac{\cos(\rho - \gamma_n) \cdot \tau_\Phi}{\sin\Phi \cdot \cos(\Phi + \rho - \gamma_n)} \cdot b \cdot h \tag{3.25}$$

$$|\vec{F}_f| = \frac{\sin(\rho - \gamma_n) \cdot \tau_\Phi}{\sin\Phi \cdot \cos(\Phi + \rho - \gamma_n)} \cdot b \cdot h \tag{3.26}$$

3.8.1.3 Calculation of the Shear Angle

KRYSTOF developed a model for the simple calculation of the shear angle [Krys39]. He made the following assumptions:

- The theory of the shear plane is valid.
- The maximum shear stress leads to material collapse.

In the main axial system, maximum shear stresses occur at an angle of 45°. For calculations of the cutting process, the position of the main axial system is assumed to be approximately in the direction of the resulting contact stress (Fig. 3.51).

For purposes of simplicity, the principle stress is not represented by the stress tensor but simply by vector addition. In this case, the friction angle approximates the orientation of the main axial system.

The function relation between the shear angle, the tool orthogonal rake angle and the friction angle can be derived from Fig. 3.51. The following is valid for the shear angle:

$$\Phi = \frac{\pi}{4} - (\rho - \gamma_n) \tag{3.27}$$

MERCHANT has suggested a possibility of calculating the shear angle that makes the following assumptions [Merc45, Merc45a]:

- The theory of the shear plane is valid.
- The position of the shear plane is determined by the minimum of cutting energy.

The value of cutting force can be read off the circle of THALES in Fig. 3.50:

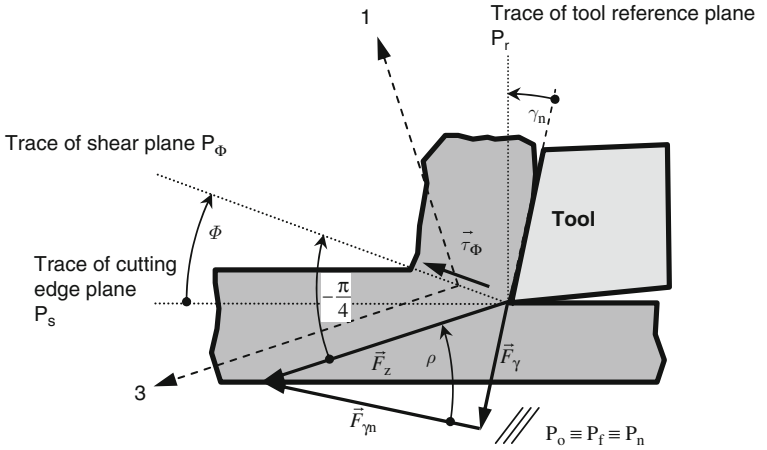

Fig. 3.51 Principle of the maximum shear stress, acc. to KRYSTOF [Krys39]

$$|\vec{F}_c| = \frac{\cos(\rho - \gamma_n)}{\cos(\Phi + \rho - \gamma_n)} \cdot \frac{b \cdot h}{\sin\Phi} \cdot \tau_\Phi \tag{3.28}$$

The necessary and the sufficient conditions for calculating the position of the energy minimum are

$$\text{nec.:}\ \frac{\partial E_c}{\partial \Phi} = 0 \qquad \text{suff.:}\ \frac{\partial^2 E_c}{\partial \Phi} \neq 0 \tag{3.29}$$

Since the cutting energy is calculated as the product of the cutting force and the cutting path, and the cutting path is not a function of the shear angle, we can simplify to:

$$\text{nec.:}\ \frac{l_c \cdot \partial|\vec{F}_c|}{\partial \Phi} = 0 \qquad \text{suff.:}\ \frac{\partial^2|\vec{F}_c|}{\partial \Phi} \neq 0 \tag{3.30}$$

From which follows for the shear angle:

$$\Phi = \frac{\pi}{4} - \frac{1}{2} \cdot (\rho - \gamma_n) \tag{3.31}$$

3.8.2 Application of Plasticity Theory to Cutting

HUCKS and OPITZ developed a shear angle equation by applying MOHR's slip theory to the orthogonal cutting process [Huck51, Opit53, Mohr06]. As opposed to the models of KRYSTOF and MERCHANT, this theory makes it possible to take a material-specific slip angle into consideration instead of an idealized 45°. It should

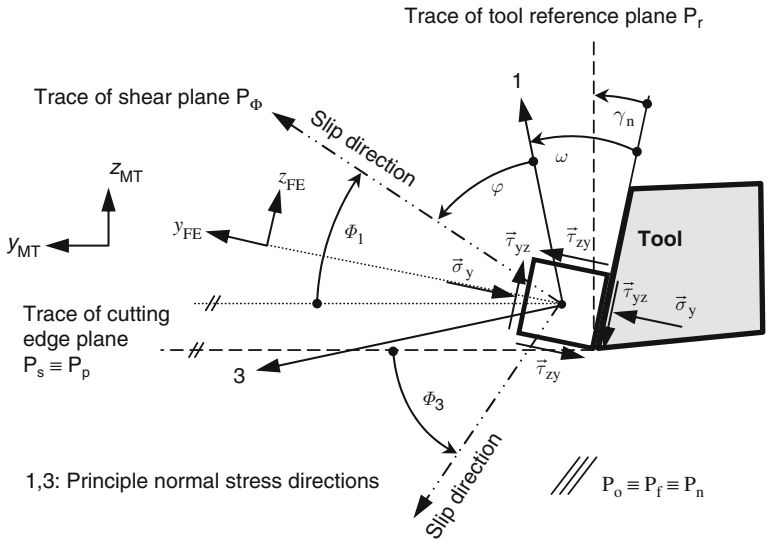

Fig. 3.52 Surface element at the cutting part, acc. to HUCKS [Huck51]

again be pointed out that the previously known shear angle need not necessarily be equal to the angle given by the actual position of the slip surface, since the direction of the shear plane was previously only purely geometrically determined by ideal considerations. In this case the directional angle of the slip surface towards the tool cutting edge plane is designated as the shear angle Φ. First a square surface element is considered on the rake face that experiences both shear and compressive stresses from the tool (Fig. 3.52).

The shear stresses also appear on all remaining faces of the quadratic element as a result of the law of equality of shear stress. Due to the unhindered flow of the chip over the face there is a very small amount of compressive stress in this direction, which will be neglected in the following. There are therefore two compressive stresses and four shear stresses on the surface element under consideration.

If we now determine the principle normal stress with the help of MOHR's stress circle, we establish the validity of the following equation:

$$\omega = \frac{1}{2} \arctan(2 \cdot \mu) \tag{3.32}$$

The angle between the rake face and the principle stress direction is thus determined by the friction coefficient between the rake face and the chip. This relation makes it clear, for example, why different cutting speeds yield different shear angles. The friction coefficient is dependent on the cutting speed and consequently alters the principle stress direction. The slip direction on the other hand is inclined towards the principle stress directions by a materially dependent angle φ. This angle can be

calculated from the compressive flow stress σ_D and the shear flow stress τ_F with the help of flow tests and MOHR's stress circle:

$$\varphi = 45 - \frac{1}{2}\arcsin\left(\frac{\sigma_D - 2\tau_F}{\sigma_D}\right) \tag{3.33}$$

For an ideal plastic body which is approximately realized by steel at the yielding point, the flow plane is under 45° in relation to the principle stress direction, since there the shear stress is at a maximum [Huck51].

With this, we obtain the principle stress and slip directions shown in Fig. 3.52 relative to the rake face. With the help of the angles γ, φ, and ω, the slip angle Φ_1 can now be calculated:

$$\Phi_1 = \varphi - \frac{1}{2}\arctan(2\mu) + \gamma_n \tag{3.34}$$

Slip angle Φ_3 is in the still undeformed area, which is why only slip angle Φ_1 (which is identical with the shear angle) is significant. The shear angle calculated here presumes an extrapolation of the stress conditions via the shear plane and the width of flank wear land as well as the formation of a continuous chip. This approximation was proven to be in accordance with experiments made on materials with envelope lines that are inclined and parallel to the σ-axis. HUCKS did not experiment with materials with bent envelope curve [Huck51].

With the help of the shear angle, the resultant forces can now also be calculated. To do this, the stresses that are active in the shear plane are multiplied with shear plane surface, resulting in a normal and tangential force in the shear plane. We will in this context proceed without the derivation of HUCKS's formulae. For steel, which has an envelope line that is parallel to the σ-axis, the following formulae for cutting and feed force result with width of undeformed chip b and chip thickness h according to HUCKS:

$$F_c = \tau_0 \cdot b \cdot h \cdot \left[\frac{1}{2\sqrt{\mu^2 + \frac{1}{4}}} + \cot g(\phi)\right] \tag{3.35}$$

$$F_f = \tau_0 \cdot b \cdot h \cdot \left[\frac{\cot g(\phi)}{2\sqrt{\mu^2 + \frac{1}{4}}} - 1\right] \tag{3.36}$$

To sum up, we can say that the highly numerous experimental relations in chip formation depend only on a few numbers of materials and the friction coefficient. HUCKS's work made the fundamentally new discovery that the stress field in the chip on the cutting edge depends, besides its intensity, only on the friction coefficient and the normal direction of the envelope line [Huck51].